Fluid Phase Equilibria 509 (2020) 112444

Contents lists available at ScienceDirect

Fluid Phase Equilibria

journal homepage: www.elsevier.com/locate/fluid

Thermodynamics of the carbon dioxide plus nitrogen plus methane ($CO_2 + N_2 + CH_4$) system: Measurements of vapor-liquid equilibrium data at temperatures from 223 to 298 K and verification of EOS-CG-2019 equation of state

Sindre Ottøy [a, b], Tobias Neumann [b, c], Hans Georg Jacob Stang [a], Jana Poplsteinova Jakobsen [b], Anders Austegard [a], Sigurd Weidemann Løvseth [a, *]

[a] SINTEF Energy Research, Postboks 4761 Torgarden, NO-7465, Trondheim, Norway
[b] Norwegian University of Science and Technology (NTNU), NO-7491, Trondheim, Norway
[c] Thermodynamics, Ruhr-Universität Bochum, Universitätsstraße 150, 44801, Bochum, Germany

ARTICLE INFO

Article history:
Received 1 October 2019
Received in revised form
8 December 2019
Accepted 21 December 2019
Available online 27 December 2019

Keywords:
Phase equilibrium
Measurements
Fundamental equation of state
Carbon dioxide
Nitrogen
Methane
CO2 capture and storage

ABSTRACT

Vapor-liquid equilibria (VLE) data of the ternary mixture of $CO_2 + N_2 + CH_4$ were measured at the isotherms 223 K, 253 K, 273 K, 283 K, and 298 K and for pressures in the range of 0.8 MPa–9.3 MPa. The 62 experimental dew or bubble point data points have been measured using an analytical technique. For each temperature, the ratio between N_2 and CH_4 mole fraction in the total composition has been close to constant, enabling the data to be visualized as quasi phase envelopes. Estimated standard measurement uncertainties ($k = 1$) better than 14 mK in temperature, 1.5 kPa in pressure, and 0.06 mol% in composition are reported, yielding a total uncertainty in terms of composition better than 0.07 mol%. The experimental data were compared to the EOS-CG-2019 model, which is a state-of-the-art Helmholtz energy-based equation of state for the mixture of $CO_2 + N_2 + CH_4$. All deviations between model and experimental data points are below 0.5 mol% for liquid compositions and 1.0 mol% for vapor compositions. The deviations between model and experimental points in the ternary mixture of $CO_2 + N_2 + CH_4$ follow the same trends seen in earlier reports between model and experimental data for the binary mixtures of $CO_2 + N_2$ and $CO_2 + CH_4$. In addition, the model was analysed with respect to other thermophysical properties available in the literature. To a large extent, the results presented in this work validate the assumption that the thermodynamic properties of the multicomponent system $CO_2 + N_2 + CH_4$ can be described purely based on the pure component and binary mixture contributions.

1. Introduction

The fluid properties of CO_2 mixed with other components are receiving intensified interest due to the need of reducing anthropic global warming. Carbon capture and storage (CCS) will be a vital technology in order to avoid the catastrophic consequences of global climate change caused by continued largely unchecked emissions of CO_2 and other greenhouse gases (GHG) to the atmosphere. This view is strongly supported by recent international studies [1–3]. As a step-stone to global large-scale CCS, further industrially driven projects are currently under planning. One of these is the Norwegian Full-Scale project [4], where CO_2 emissions from industrial point sources will be captured, liquefied, transported by ship to a coastal terminal close to a reservoir suitable for storage to which the CO_2 will be transported by pipeline.

In order to avoid a slow-down of CCS deployment, it is of vital importance that such early projects are safe, technologically robust, and not excessively expensive in investments and operation. Thermodynamic models of high quality are necessary to fulfill these requirements, which again will depend on experimental data of high quality for development and verification [5]. Currently, the thermodynamic equilibrium properties of pure CO_2 are known to relatively high degree of accuracy [6,7].

However, in real CCS-systems, the CO_2 will never be completely

* Corresponding author.
E-mail address: Sigurd.w.loevseth@sintef.no (S.W. Løvseth).

https://doi.org/10.1016/j.fluid.2019.112444

pure, and even small amounts of impurities can cause considerable changes in fluid properties, in particular regarding phase equilibria, with possibly detrimental impacts. For instance, in most systems, it would be a priority to avoid corrosion caused by the presence of a water-rich phase, which, depending on temperature and pressure, occurs even for minute concentrations of water, in particular in the presence of other impurities [8–10]. At lower temperatures hydrates can form that potentially can plug systems at even lower water concentrations [11–13]. In general, the presence of non-condensable gases, will lead to increased compression and transportation costs and higher operating and dimensioning pressures [14,15].

Despite the continuing progress of molecular dynamics, the high complexity of physical interactions in multicomponent mixtures still require fitting of thermodynamic models to experimental data in order to get satisfactory accuracy. Thermodynamic models in terms of the Helmholtz-energy for mixtures are built up by combining models for the individual pure components with binary mixture terms. The multicomponent mixture is normally not fitted, mainly because a full experimental mapping of all relevant conditions for such mixtures in practice is impossible. However, all models should be checked against multicomponent data to verify their performance against real operating conditions.

Unfortunately, the data situation, and hence reliability of thermodynamic models, is not satisfactory for CO_2 mixed with a number of relevant impurities [5,16,17]. Unless the data and model situation is improved, the risk associated with the corresponding uncertainty in fluid properties can only be mitigated through the use of excessive safety margins in design, specifications, causing higher costs and energy consumption than necessary.

Hence, in order to address the current perceived cost and risk barriers associated with CCS, SINTEF Energy Research, the Norwegian University of Science and Technology, and the Ruhr-Universität Bochum have over the last decade made a considerable effort to improve the knowledge of thermodynamic properties relevant for CCS through multiple projects [15,18,19]. This collaboration is currently facilitated mainly through the Norwegian CCS Research Centre [19]. The work has included both development of thermodynamic models and measurements of equilibrium properties of relevant mixtures, with the EOS-CG equation of state (EOS) [16,20–23] and a purpose-built and highly accurate analytical phase equilibrium facility called CO_2Mix [24,25] being important work horses. The EOS-CG-2019 [16] is a highly accurate [17] Helmholtz energy-based reference EOS, which currently includes the most important components relevant for CCS and is continually improved. The CO_2Mix facility has provided new and accurate phase equilibrium data for binary mixtures of CO_2 and N_2, O_2, CH_4, Ar, and CO [21,25–29]. Both EOS-CG-2019 and CO_2Mix are central to the current work and will hence be discussed in further detail below.

As discussed above, an assumption for most EOS like EOS-CG-2019 is that multi-component mixtures can be described purely based on models for the pure components and all possible binary combinations. However, little work has been executed so far to verify this approach for CO_2-rich mixtures. The aim of the present work has been to investigate the thermodynamics of the ternary system $CO_2 + N_2 + CH_4$. Nitrogen and methane are generally considered to be among the most central impurities within CCS [30–32]. Nitrogen is normally an important component in the exhaust gas which is partly carried through to the enriched CO_2 for many capture processes. Methane could be an important impurity resulting from gas sweetening or pre-combustion capture processes. In addition, methane and CO_2 mixtures are found in reservoirs, naturally or when CO_2 is injected for enhanced oil (EOR) or gas (EGR) recovery. Compared with the other binary mixtures relevant for CCS, the amount of experimental data on the thermodynamics of $CO_2 + N_2$ and $CO_2 + CH_4$ binary systems is rather extensive. For these two systems, the binary mixture models [33] developed for the GERG EOS [33,34] are used in the EOS-CG-2019. But instead of using simpler EOSes for the pure components as done in GERG, the reference EOSes are employed in EOS-CG-2019 [16,35]. Although large deviations are found between some of the $CO_2 + CH_4$ and $CO_2 + N_2$ binary data, and the critical region is not described accurately [25,28], the data situation for $CO_2 + CH_4$ and $CO_2 + N_2$ mixtures is in general considered good and the GERG mixture models have high accuracy at technology relevant low impurity levels. However, for the ternary system of $CO_2 + N_2 + CH_4$, less data are available and there is a need for a verification of the model.

In this work, new accurate vapor-liquid equilibrium (VLE) data are provided for the $CO_2 + N_2 + CH_4$ system at temperatures of 223 K, 253 K, 273 K, 283 K, and 298 K and pressures up to 9.3 MPa. Subsequently the EOS-CG-2019 is compared and verified against this new data set as well as other available experimental data from the literature.

The experimental methods are presented in Section 2 in this article. In Section 3, the experimental data and related uncertainty analysis are provided. A comparison and validation of the EOS-CG-2019 model with both the new and existing literature data of the system are discussed in Section 4. The work is concluded in Section 5.

2. Experimental methods

As mentioned above, an accurate setup developed specifically for CCS-relevant mixtures and conditions has been used in this work. The setup, shown schematically in Fig. 1, is employing an analytical isothermal method. A sapphire tube between two titanium flanges makes up the 100 ml equilibrium cell. A thermostatic bath controls the temperature of the cell. Two standard platinum resistance thermometers (SPRTs) are located in the bottom and top flange to measure the temperature and provide information about its uniformity. Pumps and valves in the top and bottom flanges are used to control cell content and total composition in the equilibrium cell. A membrane separates four absolute pressure transmitters from the cell content. The cell pressure is found by combining this array of transmitters with different full-scale values with a differential pressure sensor. A magnetic stirrer in the bottom of the cell is used to faster reach equilibrium during measurements. At nominal equilibrium conditions, the fluid phase compositions are measured by sampling and analyzing the samples in a gas chromatograph (GC) with a thermal conductivity detector (TCD). The method used for analyzing the output of the GC has been developed in-house and is further described in section 2.4.

Because the setup and methods used to calibrate the systems and obtain the vapor-liquid equilibrium (VLE) data in this work are almost identical to what have been described previously [21,24–29], further details will not be given here except for the modifications described in the following sections.

2.1. Sampling procedure

Unlike most of the previous reported measurements with this setup, no volume compensation was made for the small samples extracted from the cell. Hence, the pressure changed slightly after each sampling.

Two different strategies, which here are called alternating and sequential sampling, were used for the VLE measurements.

In the first strategy, the data points were obtained by sampling alternatingly from the liquid and vapor phase. Between each

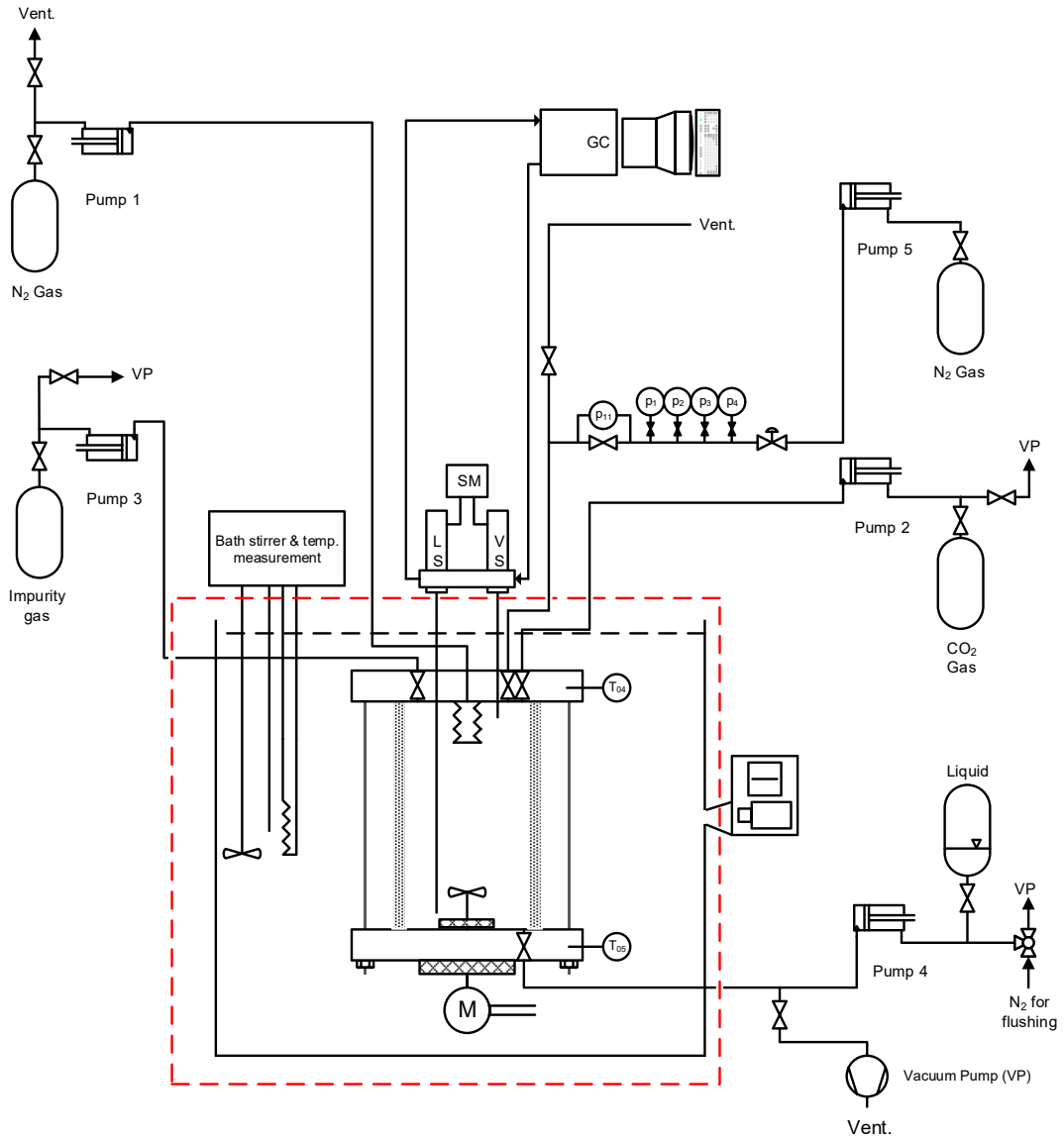

Fig. 1. Schematic diagram of experimental setup [25,27].

sample, the cell was stirred until the pressure stabilized within 1 kPa for at least 15 min. The cell content was then left to settle for at least 20 min. Since a 40-min GC program was used, the minimum time between each sample was 40 min. However, pressure stabilization was slower closer to the critical point and more stirring time was often needed. At least 6 samples were taken from each fluid phase, with the first sample considered a flushing sample.

The remainder of the data points were measured using sequential sampling. Here, each liquid data point was obtained by extracting 6 samples at 42-min intervals without stirring between each sample. The cell content was then stirred for at least 15 min until the pressure stabilized within 1 kPa and left to settle for at least 20 min. Finally, 6 samples were extracted from the vapor phase without stirring between samplings.

2.2. Source gases

Table 1 lists the source gases used to make the reference gas mixtures listed in Table 4. The source gases were also used directly in the VLE measurements. The source gases were not purified or treated any further before use. The GC used helium as a carrier gas.

2.3. Calibration of pressure and temperature sensors

Prior to the present measurements, the array of absolute pressure transmitters of the setup (Keller model PAA-33X) were calibrated using a dead-weight tester. The residuals following the calibration of the pressure transmitters used in the measurement presented here were all approximately at or below the specified precision of the transmitters. This specified precision is for all the transmitters 0.01% of full scale, and the corresponding uncertainty is hence 0.1 kPa, 0.3 kPa, and 1 kPa for the pressure transmitters with full scale reading of 1 MPa, 3 MPa, and 10 MPa, respectively.

The two standard platinum resistance thermometers (SPRTs) of the setup have been calibrated using fixed point cells as previously described in detail [25]. A recalibration was performed just prior to the current measurement, and the deviation identified was around 1 mK. This is below the overall uncertainty in temperature due to thermal inhomogeneity between the two SPRTs.

Table 1
Specifications of single component mixtures used in the experiments.

Chemical name	CAS #	Source	Purification method	Final mole fraction purity	Analysis method
Carbon dioxide	124-38-9	AGA	None	0.999993	None
Nitrogen	7727-37-9	AGA	None	0.999999	None
Methane	74-82-8	AGA	None	0.999995	None
Helium	7440-59-7	AGA	None	0.999999	None

2.4. Calibration of composition measurements

The composition measurements were calibrated using the same procedure as described in Ref. [25]. A gravimetric procedure was used to prepare the 7 reference gas mixtures listed in Table 4, with compositions known to high accuracy spanning the 2-dimensional range of composition of the phase equilibria measurements. Each of the reference gases were extracted from the cell to investigate the GC response. Both samplers were used in these calibration measurements. The sample size, and hence the area recorded in the chromatogram, was varied to span the required range needed for the phase equilibrium measurements. A series of samples were extracted for each combination of reference gas mixture, sampler, and sample size. To analyze the GC response during these calibration and later VLE measurements, a purpose-designed integration technique was used to integrate the area under the three peaks in the chromatogram of each sample, where each peak corresponded to one of the three components. The data obtained by analyzing these samples were used to construct calibration functions of similar form to what was used in Ref. [25], but optimized for and with some added complexity due to the additional component of methane:

$$\begin{aligned} k\hat{n}_{CO_2} &= A_{CO_2} + c_1 \left(A_{CO_2}\right)^{c_2} + c_3 A_{N_2}, \\ k\hat{n}_{N_2} &= c_4 A_{N_2} + c_5 \left(A_{N_2}\right)^{c_6}, \\ k\hat{n}_{CH_4} &= c_7 A_{CH_4} + c_8 \left(A_{CH_4}\right)^{c_9}, \\ \hat{y}_{i,\mathrm{cal}} &= \frac{k\,\hat{n}_i}{\sum\limits_{\substack{\mathrm{All} \\ \mathrm{comp.}}} k\hat{n}_j} = \frac{\hat{n}_i}{\sum\limits_{\substack{\mathrm{All} \\ \mathrm{comp.}}} \hat{n}_j}. \end{aligned} \tag{1}$$

Here, $\hat{y}_{i,\mathrm{cal}}$ and $\hat{n}_i$ are estimators for the mole fraction and mole number of component i in the mixtures, with i being CO_2, N_2, or CH_4. The parameters c_m with $m = 1\ldots9$ were fitted separately for the liquid and vapor sampler, using the area responses of the GC for the respective samplers. The parameters were fitted separately for the liquid and vapor sampler for the same reasons as given in Petropoulou et al. [28]. A least squares approach was used to fit the optimal parameters, minimizing the objective function given below:

$$S(\boldsymbol{c}) = \sum_{\mathrm{series}} W_s \sum_{\substack{\mathrm{All} \\ \mathrm{comp.}}} \left(\frac{y_{j,\mathrm{cal}} - \bar{\hat{y}}_{j,\mathrm{cal},s}}{\sqrt{u_c^2\left(y_{j,\mathrm{cal}}\right) + s^2\left(\bar{\hat{y}}_{j,\ \mathrm{cal},s}\right)}} \right)^2. \tag{2}$$

Here, $y_{j,\mathrm{cal}}$ is the mole fraction of component j determined in the gravimetric analysis, $\bar{\hat{y}}_{j,\mathrm{cal},s}$ is the predicted average mole fraction and $s^2(\bar{\hat{y}}_{j,\mathrm{cal},s})$ is the variance of the predicted average mole fraction of component j in the given series s, and $u_c(y_{j,\mathrm{cal}})$ is the combined standard uncertainty in the mole fraction of component j of the gravimetrically prepared reference mixtures. Each series summed over consisted of 5 repetitions with approximately the same area output of the GC. Hence, the series with low uncertainties and low variances were weighted higher in the optimization. The weighing factor W_s of equation (2) allows for individual weighing of the different gravimetrically prepared mixtures in the optimization, as described in Section 3.2.2.

3. Experimental results and uncertainty analysis

3.1. Summary of data

The new bubble and dew point data of the current work are provided in Tables 2 and 3, respectively. The same data are plotted in Fig. 9 and Figs. A.3 to A.6. The standard combined uncertainty [36] in the temperature, $u_c(\overline{T}_f)$, pressure, $u_c(\overline{p}_f)$, and mole fraction of each component i, $u_c(x_{f,i})$ and $u_c(y_{f,i})$, as well as the total standard uncertainty of the bubble and dew points in terms of CO_2 mole fraction, $u_{\mathrm{tot}}(x_{f,\mathrm{CO_2}})$ and $u_{\mathrm{tot}}(y_{f,\mathrm{CO_2}})$, are stated along with the measured temperature, pressure and composition of each VLE point. A total of 31 bubble and 31 dew points are reported at the temperatures 223 K, 253 K, 273 K, 283 K and 298 K. The experimental points L1–L5, L10–L31, V1–V5 and V10–V31 were measured with approximately equal amounts of nitrogen and methane in the total composition of the cell. The experimental points L6-L9 and V6–V9 were measured with a ratio between total concentration of nitrogen (z_{N_2}) and methane (z_{CH_4}) of approximately $z_{N_2} : z_{CH_4} = 4.4 : 1$.

3.2. Composition measurement calibration

3.2.1. Reference gas mixtures

7 different reference gas mixtures were gravimetrically prepared for the calibration of the composition measurements. The estimated composition and uncertainty in composition of the gravimetrically prepared mixtures are provided in Table 4. For details on the estimation of this uncertainty, the reader is referred to previous work [21,25].

3.2.2. Fitting of calibration function

30 calibration measurements, 5 repetitions at 6 different area samplers, were taken of each of the 7 different reference mixtures using both samplers. In the fitting of parameters c_i with $i = 1\ldots9$ of equation (1) to the measurements, data from reference mixture #6 was weighed by a factor 4.5 higher in the vapor sampler calibration to eliminate a systematic trend otherwise seen in the residuals at lower CO_2 concentration. An explanation for this corrected bias could be that all the other reference mixtures had significantly higher CO_2 concentrations. The fitted parameters of equation (1) are provided in Table 5, together with the standard error of the fit, $S_E(y_i)$, for the mole fraction of the three components i of the mixture.

Residual plots of the fitted calibration measurements versus the composition are shown in Figs. 2–3. A small trend of increasing residuals in the methane mole fraction can be seen for both the liquid and vapor sampler.

Table 2
Bubble point measurements of the present work for the $CO_2 + N_2 + CH_4$ system at temperatures $\overline{T}_f$, pressures $\overline{p}_f$. x_{f,CO_2}, x_{f,N_2}, and x_{f,CH_4} are mole fractions of CO_2, N_2, and CH_4, respectively. u_c denotes the compounded standard measurement uncertainty of these different quantities. The estimated total compounded standard uncertainty of the bubble point in terms of CO_2 mole fraction is given by $u_{tot}\left(x_{f,CO_2}\right)$. The total bubble point uncertainties in terms of N_2 and CH_4 mole fraction are lower. See the main text for further details.

ID	$\overline{T}_f$	$\overline{p}_f$	x_{f,CO_2}	x_{f,N_2}	x_{f,CH_4}	$u_c(\overline{T}_f)$	$u_c(\overline{p}_f)$	$u_c(x_{f,CO_2})$	$u_c(x_{f,N_2})$	$u_c(x_{f,CH_4})$	$u_{tot}(x_{f,CO_2})$
	/K	/MPa	/-	/-	/-	/K	/MPa	/-	/-	/-	/-
L1	298.138	7.0850	0.9807	0.0089	0.0104	8.5E-03	1.5E-03	4.2E-04	3.4E-04	2.7E-04	4.2E-04
L2	298.133	7.5238	0.9651	0.0163	0.0186	5.1E-03	1.4E-03	4.2E-04	3.4E-04	2.7E-04	4.2E-04
L3	298.131	7.7887	0.9535	0.0220	0.0244	5.5E-03	1.4E-03	4.2E-04	3.4E-04	2.7E-04	4.2E-04
L4	298.131	7.9281	0.9440	0.0266	0.0294	5.8E-03	1.4E-03	4.6E-04	3.5E-04	2.8E-04	4.7E-04
L5	298.130	7.8767	0.9487	0.0246	0.0267	5.4E-03	1.4E-03	4.5E-04	3.5E-04	2.8E-04	4.6E-04
L6	298.129	6.8975	0.9885	0.0090	0.0024	4.6E-03	1.4E-03	4.2E-04	3.4E-04	2.7E-04	4.2E-04
L7	298.129	7.3045	0.9769	0.0183	0.0048	4.8E-03	1.4E-03	4.3E-04	3.5E-04	2.7E-04	4.3E-04
L8	298.129	7.6691	0.9651	0.0278	0.0071	5.8E-03	1.4E-03	4.2E-04	3.4E-04	2.7E-04	4.2E-04
L9	298.129	7.9272	0.9551	0.0362	0.0088	5.5E-03	1.4E-03	4.2E-04	3.4E-04	2.7E-04	4.3E-04
L10	283.154	5.2541	0.9803	0.0083	0.0115	1.3E-02	1.3E-03	4.2E-04	3.4E-04	2.7E-04	4.2E-04
L11	283.154	6.1461	0.9550	0.0201	0.0249	1.3E-02	1.3E-03	4.2E-04	3.4E-04	2.7E-04	4.2E-04
L12	283.154	7.0889	0.9262	0.0350	0.0388	1.3E-02	1.4E-03	4.2E-04	3.4E-04	2.7E-04	4.2E-04
L13	283.155	7.6800	0.9055	0.0449	0.0496	1.4E-02	1.4E-03	4.2E-04	3.4E-04	2.7E-04	4.2E-04
L14	283.156	8.2586	0.8831	0.0567	0.0602	1.3E-02	1.4E-03	4.2E-04	3.4E-04	2.7E-04	4.2E-04
L15	283.156	8.8483	0.8526	0.0709	0.0766	1.4E-02	1.4E-03	4.2E-04	3.4E-04	2.7E-04	4.3E-04
L16	273.168	3.9903	0.9874	0.0050	0.0076	1.0E-02	1.3E-03	4.2E-04	3.4E-04	2.7E-04	4.2E-04
L17	273.166	5.2521	0.9527	0.0195	0.0277	1.1E-02	1.3E-03	4.2E-04	3.4E-04	2.7E-04	4.2E-04
L18	273.167	6.2607	0.9226	0.0330	0.0444	9.9E-03	1.3E-03	4.2E-04	3.4E-04	2.7E-04	4.2E-04
L19	273.167	7.2203	0.8913	0.0478	0.0609	1.0E-02	1.4E-03	4.2E-04	3.4E-04	2.7E-04	4.2E-04
L20	273.167	8.1663	0.8565	0.0652	0.0783	9.6E-03	1.4E-03	4.2E-04	3.4E-04	2.7E-04	4.2E-04
L21	273.169	8.8023	0.8294	0.0794	0.0912	1.0E-02	1.4E-03	4.2E-04	3.4E-04	2.7E-04	4.2E-04
L22	273.170	9.3244	0.8031	0.0939	0.1030	1.0E-02	1.4E-03	4.2E-04	3.4E-04	2.7E-04	4.2E-04
L23	253.162	2.3369	0.9910	0.0033	0.0057	3.3E-03	5.7E-04	4.2E-04	3.4E-04	2.7E-04	4.2E-04
L24	253.162	2.6863	0.9821	0.0066	0.0113	3.5E-03	5.8E-04	4.2E-04	3.4E-04	2.7E-04	4.2E-04
L25	253.163	3.0423	0.9727	0.0102	0.0171	3.2E-03	1.3E-03	4.2E-04	3.4E-04	2.7E-04	4.2E-04
L26	253.162	3.4109	0.9629	0.0141	0.0231	3.2E-03	1.3E-03	4.2E-04	3.4E-04	2.7E-04	4.2E-04
L27	253.163	3.7991	0.9523	0.0183	0.0294	3.0E-03	1.3E-03	4.2E-04	3.4E-04	2.7E-04	4.2E-04
L28	223.151	0.7965	0.9972	0.0009	0.0018	6.7E-03	3.5E-04	4.2E-04	3.4E-04	2.7E-04	4.2E-04
L29	223.151	0.9958	0.9925	0.0024	0.0051	6.7E-03	3.5E-04	4.2E-04	3.4E-04	2.7E-04	4.2E-04
L30	223.151	1.0983	0.9899	0.0033	0.0068	6.5E-03	5.5E-04	4.2E-04	3.4E-04	2.7E-04	4.2E-04
L31	223.150	1.2246	0.9867	0.0044	0.0089	5.9E-03	5.5E-04	4.2E-04	3.4E-04	2.7E-04	4.2E-04

3.3. Estimation of the data points

As discussed in Section 2.1, no volume compensation was employed in the current work. This means that each consecutive sample was at a slightly lower pressure, and hence also the composition of each phase was shifted slightly. Similar to Ref. [21], it was assumed that the system was closest to equilibrium before the first sample at a pressure/temperature point. Hence, the average pressure measured in the 2 min before the first flushing sample defined the equilibrium data point pressure, $\overline{p}_f$. Similar to our previous work without volume compensation [21], the mole fraction of component i at the equilibrium pressure, $x_{f,i}$ *or* $y_{f,i}$, was found through linear regression using the composition and pressure measurements of samples of the data point. An example of such linear regression is shown in Fig. 4.

3.4. Temperature and pressure uncertainty and verification

The methodology of previous work [25,27] was used for each data point to estimate the systematic standard uncertainties ($k = 1$) [36] in temperature, pressure, and composition. The combined uncertainties in pressure and temperature, $u_c(\overline{p}_f)$ and $u_c(\overline{T}_f)$, are found by a root mean sum of the estimated standard deviation and systematic uncertainty, since these uncertainty contributions can be assumed independent of each other.

The uncertainties are given in Tables 2–3. The estimated temperature uncertainty is dominated by observed non-uniformity and is for most data points below 10 mK, and for all data points below 14 mK. The estimated pressure uncertainty is dominated by the precision and the calibration uncertainty of the pressure transmitters, with a maximum value among all the data points of 1.5 kPa.

The calibration in temperature and pressure and their uncertainty estimates were verified by measuring the vapor pressure of pure CO_2 at each measurement temperature. In Table 6, these measurements are summarized and compared with the model predictions of Span-Wagner EOS for pure CO_2 [6], p_{calc}, indicating that the uncertainty estimates for pressure and temperature are reasonable.

3.5. Uncertainty of composition measurements

For binary mixtures, an uncertainty stated in the mole fraction of one component will implicitly also specify the uncertainty of the other component. However, for a ternary mixture this will not be the case. Therefore, the combined uncertainty of each component, CO_2, N_2, and CH_4, was assessed independently.

The systematic measurement uncertainty in composition is in practice the uncertainty in calibration. As seen by Tables 4–5, the standard errors of the calibration function fit were orders of magnitude larger than the uncertainty of the gravimetrically prepared reference mixtures. Hence, the former is the dominating contribution to the systematic mole fraction uncertainty of each component i, $\overline{u}_c(x_i)$ and $\overline{u}_c(y_i)$ of the VLE measurements. These systematic uncertainties were specified separately for the liquid and vapor sampler calibration function. Hence, $\overline{u}_c(x_{CO_2}) = 4.2 \times 10^{-4}$ and $\overline{u}_c(y_{CO_2}) = 5.7 \times 10^{-4}$.

The combined uncertainties of the equilibrium mole fraction measurement of each data point, as given in Tables 2-3, are estimated by combining the systematic uncertainty in concentration

Table 3
Dew point measurements of the present work for the $CO_2 + N_2 + CH_4$ system at temperatures $\overline{T}_f$, pressures $\overline{p}_f$. y_{f,CO_2}, y_{f,N_2}, and y_{f,CH_4} are mole fractions of CO_2, N_2, and CH_4, respectively. u_c denotes the compounded standard measurement uncertainty of these different quantities. The estimated total compounded standard uncertainties of the dew points in terms of CO_2 mole fraction are given by $u_{tot}\left(y_{f,CO_2}\right)$. The total dew point uncertainties in terms of N_2 and CH_4 mole fraction are lower. See the main text for further details.

ID	$\overline{T}_f$	$\overline{p}_f$	y_{f,CO_2}	y_{f,N_2}	y_{f,CH_4}	$u_c(\overline{T}_f)$	$u_c(\overline{p}_f)$	$u_c(y_{f,CO_2})$	$u_c(y_{f,N_2})$	$u_c(y_{f,CH_4})$	$u_{tot}(y_{f,CO_2})$
	/K	/MPa	/-	/-	/-	/K	/MPa	/-	/-	/-	/-
V1	298.138	7.0854	0.9587	0.0215	0.0198	8.5E-03	1.5E-03	5.7E-04	4.4E-04	3.3E-04	5.8E-04
V2	298.133	7.5243	0.9373	0.0319	0.0307	5.1E-03	1.4E-03	5.7E-04	4.4E-04	3.3E-04	5.7E-04
V3	298.131	7.7892	0.9295	0.0356	0.0350	5.5E-03	1.4E-03	5.7E-04	4.4E-04	3.3E-04	5.7E-04
V4	298.131	7.9286	0.9296	0.0350	0.0353	5.8E-03	1.4E-03	5.7E-04	4.4E-04	3.3E-04	5.7E-04
V5	298.130	7.8772	0.9285	0.0359	0.0356	5.4E-03	1.4E-03	5.7E-04	4.4E-04	3.3E-04	5.7E-04
V6	298.129	6.8978	0.9710	0.0240	0.0050	4.6E-03	1.4E-03	5.7E-04	4.4E-04	3.3E-04	5.7E-04
V7	298.129	7.3050	0.9493	0.0419	0.0088	4.8E-03	1.4E-03	5.7E-04	4.4E-04	3.3E-04	5.7E-04
V8	298.129	7.6696	0.9348	0.0539	0.0112	5.8E-03	1.4E-03	5.7E-04	4.4E-04	3.3E-04	5.7E-04
V9	298.129	7.9277	0.9285	0.0593	0.0122	5.5E-03	1.4E-03	5.7E-04	4.4E-04	3.3E-04	5.7E-04
V10	283.154	5.2542	0.9110	0.0476	0.0415	1.3E-02	1.3E-03	5.7E-04	4.4E-04	3.3E-04	6.1E-04
V11	283.154	6.1439	0.8354	0.0905	0.0741	1.3E-02	1.3E-03	5.7E-04	4.4E-04	3.3E-04	6.0E-04
V12	283.155	7.0836	0.7822	0.1229	0.0949	1.3E-02	1.4E-03	5.7E-04	4.4E-04	3.3E-04	5.9E-04
V13	283.155	7.6738	0.7597	0.1334	0.1068	6.8E-03	1.4E-03	5.7E-04	4.4E-04	3.3E-04	5.7E-04
V14	283.155	8.2636	0.7463	0.1359	0.1179	1.4E-02	1.4E-03	5.8E-04	4.4E-04	3.4E-04	6.0E-04
V15	283.155	8.6818	0.7432	0.1360	0.1208	1.4E-02	1.4E-03	5.7E-04	4.4E-04	3.3E-04	5.9E-04
V16	273.167	3.9894	0.9134	0.0465	0.0401	1.0E-02	1.3E-03	5.8E-04	4.4E-04	3.3E-04	6.3E-04
V17	273.166	5.2508	0.7663	0.1263	0.1073	1.0E-02	1.3E-03	5.7E-04	4.4E-04	3.3E-04	6.0E-04
V18	273.166	6.2599	0.6967	0.1645	0.1389	1.0E-02	1.3E-03	5.7E-04	4.4E-04	3.3E-04	5.9E-04
V19	273.167	7.2129	0.6549	0.1875	0.1575	9.7E-03	1.4E-03	5.7E-04	4.4E-04	3.3E-04	5.8E-04
V20	273.168	8.1578	0.6319	0.2001	0.1679	9.6E-03	1.4E-03	5.7E-04	4.4E-04	3.3E-04	5.8E-04
V21	273.170	8.7900	0.6267	0.2021	0.1712	1.0E-02	1.4E-03	5.7E-04	4.4E-04	3.3E-04	5.8E-04
V22	273.170	9.3076	0.6301	0.1995	0.1704	1.0E-02	1.4E-03	5.7E-04	4.4E-04	3.3E-04	5.8E-04
V23	253.162	2.3336	0.8774	0.0668	0.0558	3.2E-03	5.7E-04	6.0E-04	4.5E-04	3.4E-04	6.2E-04
V24	253.162	2.6825	0.7843	0.1184	0.0973	3.2E-03	5.8E-04	5.7E-04	4.4E-04	3.3E-04	5.9E-04
V25	253.163	3.0413	0.7136	0.1575	0.1288	3.2E-03	1.3E-03	6.0E-04	4.7E-04	3.3E-04	6.4E-04
V26	253.162	3.4091	0.6566	0.1893	0.1541	3.2E-03	1.3E-03	5.7E-04	4.4E-04	3.3E-04	6.0E-04
V27	253.162	3.7969	0.6102	0.2153	0.1745	3.4E-03	1.3E-03	5.7E-04	4.4E-04	3.3E-04	5.9E-04
V28	223.151	0.7963	0.8734	0.0708	0.0558	6.7E-03	3.5E-04	5.9E-04	4.5E-04	3.4E-04	7.1E-04
V29	223.151	0.9948	0.7145	0.1606	0.1249	6.5E-03	3.5E-04	5.8E-04	4.5E-04	3.4E-04	6.5E-04
V30	223.150	1.0973	0.6537	0.1950	0.1514	6.4E-03	5.5E-04	5.8E-04	4.5E-04	3.3E-04	6.6E-04
V31	223.151	1.2233	0.5937	0.2289	0.1774	6.1E-03	5.5E-04	5.7E-04	4.4E-04	3.3E-04	6.3E-04

Table 4
$CO_2 + N_2 + CH_4$ calibration gas mixtures with estimated standard uncertainty in mole fractions $u_c\left(y_{,cal}\right)$.

Mixture #	$y_{CO_2,cal}$	$y_{N_2,cal}$	$y_{CH_4,cal}$	$u_c(y_{,cal})$
1	0.946202	0.026235	0.027563	8.9e-6
2	0.779538	0.023602	0.196858	6.8e-6
3	0.781825	0.194323	0.023850	7.1e-6
4	0.876690	0.100485	0.022825	8.1e-6
5	0.796861	0.099939	0.103199	7.2e-6
6	0.595368	0.200607	0.204021	6.8e-6
7	0.869339	0.025740	0.104920	9.4e-6

$\overline{u}_c(z_i)$ of component i with the estimator of the standard deviation of the regression $s(z_{f,i})$ at the equilibrium pressure:

$$u_c\left(z_{f,i}\right) = \sqrt{\overline{u_c}\,(z_i)^2 + s\left(z_{f,i}\right)^2} \tag{3}$$

Here and later, z is used instead of x for the liquid phase and y for the vapor phase, respectively. For most of the measurements $s(z_{f,i})$ was less than 5×10^{-5} in mole fraction and had very little impact on $u_c(z_{f,i})$.

The composition calibration was performed before the VLE measurements. However, in addition, reference mixture 2 and 4 were analysed after the new VLE data were recorded using both the vapor and liquid sampler. Almost all verification measurements were within $\overline{u}_c\,(z_i)$, and the calibration function is therefore believed to have been valid throughout the VLE measurement campaign.

Table 5
Fitted parameters to the composition calibration functions given in equation (1), as well as the standard error of this fit in terms of mole fraction, $S_E(y_i)$ with i being one of the three components CO_2, N_2, or CH_4.

Parameter	Liquid sampler	Vapor sampler
c_1	2.782×10^{-7}	1.058×10^{-7}
c_2	1.569	1.616
c_3	1.443	1.722
c_4	1387.681	1219.920
c_5	9.07×10^{-4}	9.55×10^{-4}
c_6	1.355	1.374
c_7	7.400	6.595
c_8	1.174×10^{-3}	1.174×10^{-3}
c_9	−6.220	−6.898
$S_E(y_{CO_2})$	4.2×10^{-4}	5.7×10^{-4}
$S_E(y_{N_2})$	3.4×10^{-4}	4.4×10^{-4}
$S_E(y_{CH_4})$	2.7×10^{-4}	3.3×10^{-4}

3.5.1. Total uncertainty

As in previous works [21,25,27–29], it has been found most meaningful to express the total uncertainty of the measurements in terms of composition, as expressed by:

$$u_{tot}\left(z_{f,i}\right) = \sqrt{\left(u_c\left(z_{f,i}\right)\right)^2 + \left(u_c\left(\overline{T}_f\right)\frac{\partial z_{f,i}}{\partial T}\right)^2 + \left(u_c\left(\overline{p}_f\right)\frac{\partial z_{f,i}}{\partial p}\right)^2}. \tag{4}$$

The partial derivatives with respect to temperature and pressure were computed numerically using the EOS-CG-2019 model. For all the measurements, the total uncertainty of CO_2 was higher than the

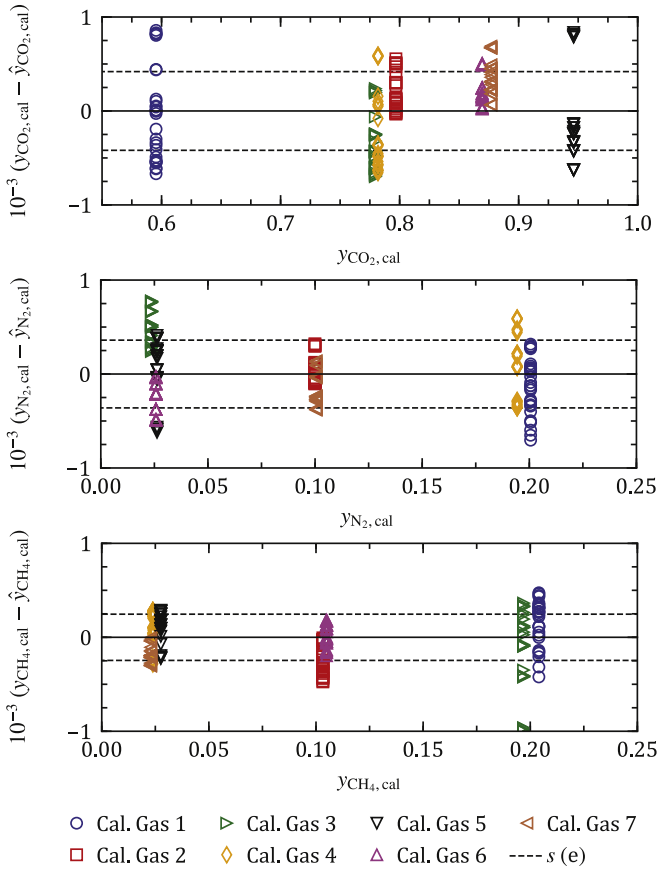

Fig. 2. Residuals between fitted composition calibration function for the liquid sampler, $\hat{\boldsymbol{y}}_{i,\mathbf{cal}}$, and the gravimetrically determined fraction, $\boldsymbol{y}_{i,\mathbf{cal}}$, of the 7 calibration gases plotted versus mole fraction of $\boldsymbol{i}$ =CO_2 (top), N_2 (middle) and CH_4 (bottom).

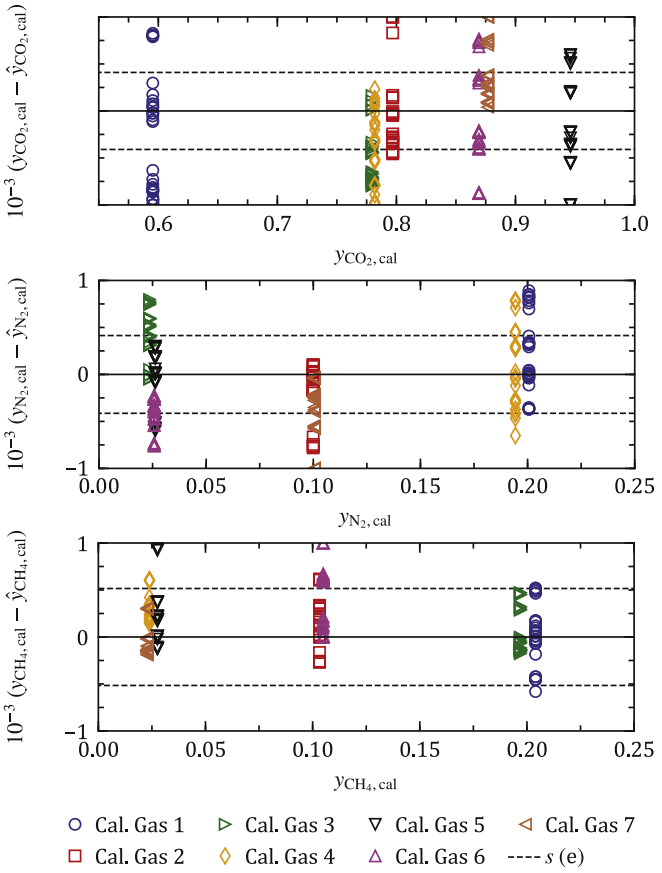

Fig. 3. As Fig. 2, but for the vapor sampler.

total uncertainty of methane and nitrogen. This was mainly due to higher combined uncertainty in the mole fraction of CO_2, $u_c(z_{f,CO_2})$, and higher partial derivatives with respect to pressure, $\frac{\partial z_{f,CO_2}}{\partial p}$. The values provided for $u_{tot}(z_{f,CO_2})$ in Tables 2 and 3 are hence also conservative estimates for $u_{tot}(z_{f,N_2})$ and $u_{tot}(z_{f,CH_4})$ which have been omitted from the tables for simplicity.

As in previous works using this facility, the composition calibration uncertainty dominates the total uncertainty. Hence, for both the bubble and dew points, the variation in total uncertainty in terms of CO_2 mole fraction is small. In all cases the uncertainties are at or below 5×10^{-4} for the bubble points and 7×10^{-4} for the dew points.

4. Analysis, data review, and comparison between the EOS-CG-2019 model and available data

4.1. Fundamental equation of state

Since there was no new equation of state developed in this work, only the general structure of the ternary model is briefly discussed in the following.

The model is defined in terms of the reduced Helmholtz energy α with the independent state variables density ρ, temperature T, and the molar composition $\vec{z}$. The general structure is divided into two parts:

$$\begin{aligned}\frac{a(\rho,T,\vec{z})}{RT} &= \alpha(\delta,\tau,\vec{z}) \\ &= \alpha^{o}(\delta_{0,i},\tau_{0,i},\vec{z}) + \alpha^{r}(\delta,\tau,\vec{z}),\end{aligned} \tag{5}$$

where R is the universal gas constant [37]. Temperature and density of the ideal-gas part α^o and the residual part α^r are either reduced with the pure fluid critical parameters of the corresponding component i in a mixture of N pure fluids

$$\delta_{0,i} = \frac{\rho}{\rho_{c,i}} \quad \text{and} \quad \tau_{0,i} = \frac{T_{c,i}}{T}, \tag{6}$$

or with so-called reducing functions $\rho_r(\vec{z})$ and $T_r(\vec{z})$.

$$\delta = \frac{\rho}{\rho_r(\vec{z})} \text{ and } \tau = T_r\frac{(\vec{z})}{T}. \tag{7}$$

These functions depend on the composition of the mixture, the critical parameters of the pure fluids, and binary interaction parameters:

$$\rho_r = f\left(\vec{z},\rho_{c,i},\beta_{v,ij},\gamma_{v,ij}\right), \tag{8}$$

$$T_r = f\left(\vec{z},T_{c,i},\beta_{T,ij},\gamma_{T,ij}\right), \tag{9}$$

where β_{ij} and γ_{ij} are adjustable parameters for each involved binary mixture. A detailed description of those functions can be found in the GERG [33,34], the EOS-CG [16,38], or the EOS-LNG [39].

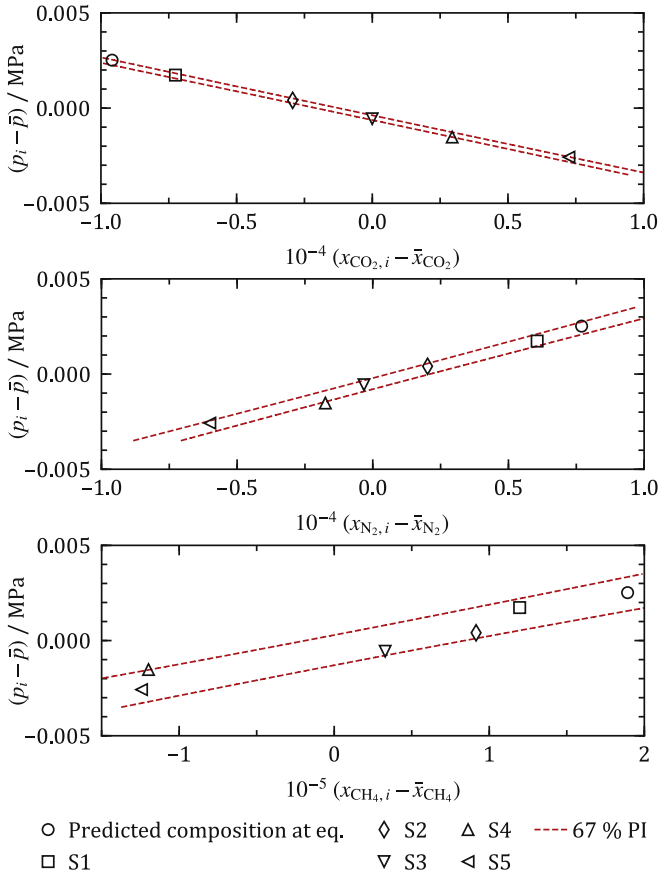

Fig. 4. Example of a linear extrapolation to determine the equilibrium mole fraction of each component. 67% confidence interval of the regression prediction is indicated by the red dashed curves. p_j and $x_{j,i}$ is the pressure and mole fraction, respectively, of sample number i (Si) and component j..

The ideal part of Eq. (5) is defined as:

$$\alpha^{o}(\rho, T, \vec{z}) = \sum_{i=1}^{N} z_i \left[\alpha^{o}_{0,i}(\delta_{0,i}, \tau_{0,i}) + \ln z_i\right]. \tag{10}$$

$\alpha^{o}_{0,i}$ are contributions from the pure-fluid equations of state for the corresponding component i in a mixture of N pure fluids. The residual contribution α^{r} describes molecular interactions in the real mixture:

$$\alpha^{r}(\delta, \tau, \vec{z}) = \sum_{i=1}^{N} z_i \alpha^{r}_{0,i}(\delta, \tau) + \Delta\alpha^{r}(\delta, \tau, \vec{z}), \tag{11}$$

where $\alpha^{r}_{0,i}$ are the residual parts calculated with the pure-fluid equations of state. For this particular ternary mixture, the departure term $\Delta\alpha^{r}$ is:

$$\begin{aligned}\Delta\alpha^{r}(\delta, \tau, \vec{z}) &= z_{CO_2} z_{CH_4} \alpha^{r}_{CO_2,CH_4}(\delta, \tau) \\ &+ z_{CO_2} z_{N_2} \alpha^{r}_{CO_2,N_2}(\delta, \tau) \\ &+ z_{N_2} z_{CH_4} \alpha^{r}_{N_2,CH_4}(\delta, \tau).\end{aligned} \tag{12}$$

The departure functions α^{r}_{ij} contain different term types with various adjustable parameters. The structures of the terms are mainly empirical.

In Eq. 10–12, it becomes evident that equations for multicomponent mixtures in terms of the Helmholtz energy are summations of pure-fluid and binary interaction contributions weighted by the composition of the mixture. The ternary equation of state investigated in this work comprises the models listed in Table 7.

4.2. Data review and analysis and comparison with EOS-CG 2019

The EOS described in Section 4.1 is validated by comparison to experimental data. For this ternary mixture, the vapor-liquid-equilibrium data measured in this work as well as in the literature are considered. The deviations between the experimental data points and the EOS are calculated in an absolute manner with respect to VLE data:

$$Z = 100\left(z_{exp} - z_{calc}\right) \tag{13}$$

and in a relative manner in terms of density data:

$$Z = 100\left(\frac{\rho_{exp} - \rho_{calc}}{\rho_{exp}}\right). \tag{14}$$

The values subscripted with “calc” are calculated with the equations listed in Table 7 and implemented in the thermophysical property software TREND [42]. For the evaluation of the whole datasets, the average absolute relative deviation (AAD) can be written as

$$\mathrm{AAD} = \frac{1}{N}\sum_{i=1}^{N} |Z_i| \tag{15}$$

where N corresponds to the number of data points in one dataset. Clear outliers are not considered in this calculation.

A summary of the available thermodynamic property data and

Table 6
Measurements of CO_2 saturation pressure ($\bar{p}$) at the temperatures ($\bar{T}$) investigated in this work. Model estimates using the EOS of Span-Wagner [6], p_{calc}, at the same temperatures are included for comparison, as well as the estimated combined uncertainty of the temperature ($u_c(\bar{T})$) and pressure ($u_c(\bar{p})$) measurements and the total VLE measurement uncertainty in terms of pressure ($u_{tot}(\bar{p})$).

ID	$\bar{T}$/K	$\bar{p}$/MPa	$p_{calc}(\bar{T})$/MPa	$u_c(\bar{T})$/K	$u_c(\bar{p})$/MPa	$u_{tot}(\bar{p})$/MPa	$(\bar{p} - p_{calc})$/MPa
P1	223.150	0.6824	0.6823	6.0E-03	3.5E-04	3.8E-04	−8.81E-05
P2	253.160	1.9695	1.9703	2.7E-03	5.7E-04	5.8E-04	8.34E-04
P3	273.168	3.4900	3.4868	1.2E-02	1.3E-03	2.1E-03	−3.24E-03
P4	283.194	4.5083	4.5071	1.0E-03	1.3E-03	1.4E-03	−1.22E-03
P5	298.148	6.4376	6.4339	3.1E-03	1.4E-03	2.5E-03	−3.64E-03

Table 7
Pure-fluid and binary-mixture EOS of the ternary model investigated in this work.

Pure-fluid EOS	Reference
CO_2	Span and Wagner [6]
CH_4	Setzmann and Wagner [40]
N_2	Span et al. [41]
Binary-mixture EOS	
$CO_2 + CH_4$	Kunz et al. [33]
$CO_2 + N_2$	Kunz et al. [33]
$N_2 + CH_4$	Kunz et al. [33]

the corresponding AAD is given in Table 8.

4.2.1. Comparisons to vapor-liquid-equilibrium data

The VLE data presented in this work and published previously by other authors are used in the following section to validate the EOS.

Since the phase boundaries are typically quite steep resulting in large $(\partial p/\partial z)_T$, deviations in terms of pressure can be become large or are not calculable. Thus, deviations in terms of composition are more meaningful and are solely shown in this work. However, in a ternary mixture it is not trivial and explicit to calculate the deviations in terms of composition in the same manner as for binary mixtures. In a binary system, the flash routines, for example included in TREND could be used with the experimental pressure and temperature, as well as any composition within in the two-phase region as inputs to calculate the corresponding points on the phase boundary and their compositions.

In a ternary mixture, the input composition for the flash calculation at a fixed pressure and temperature cannot be chosen arbitrarily within the two-phase region to calculate the same solution. Only compositions on the same tie-line lead to the same saturation point. If the experimental data point is not within the two-phase region of the model, the closest tie line has to be found in order to calculate the corresponding saturation point. Therefore, a hypothetical tie-line was drawn between the composition of the experimental saturation point in the vapor phase and in the corresponding liquid phase. This line lies consequently in the $z_{CO_2} - z_{CH_4} - z_{N_2}$-space. Starting from the experimental saturation point a small step inwards the two-phase region along that line gives the composition of the flash algorithm. The step was chosen as small as occasional convergence problems allowed it. This procedure is shown in Fig. 5 in a cutout of a ternary phase diagram with two exemplary data points. If the temperature or pressure are not exactly the same for the both phases the flash compositions are found in the same manner, but the flash is performed with the corresponding pressure and temperature. This can be done because the pressure or temperature discrepancies are small and the tie-line does not change significantly. It has to be noted that as a result of this procedure, the bubble- and dew-point compositions of the EOS are calculated with different tie lines, cf. Fig. 5, and the calculated deviations depend on the chosen step. However, those effects are neglectable because flash calculations are not unique and depend for example on chosen iteration procedures or step sizes. This method was chosen because it conserves more of the physical meaning of the residual. In contrast, the method of the shortest distance would require to use non-dimensional forms of the variables T, p, z_{CO_2}, z_{N_2}, and z_{CH_4}.

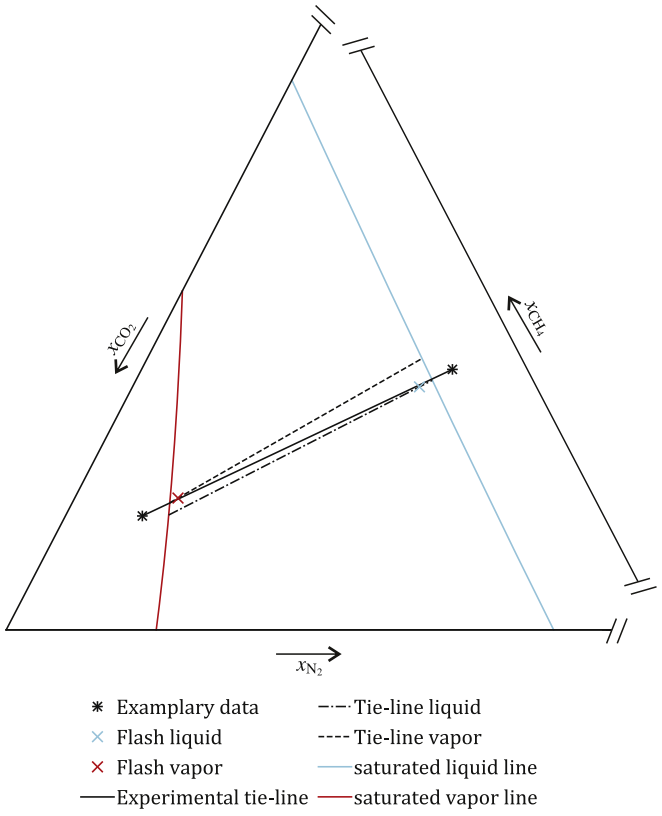

Fig. 5. Cutout of an exemplary ternary phase diagram including a qualitative visualization of the procedure to calculate deviations of VLE data.

Table 8
Overview of the available thermodynamic property data and the average absolute relative deviation (AAD) calculated with the corresponding new equation of state. AAD_x, AAD_y, x and y are given with respect to the percentage mole fraction of CO_2.

VLE data								
Authors	Year	N	T/K	p/MPa	x_{co_2}	y_{co_2}	AAD_x/%	AAD_y/%
Al-Sahhaf et al. [43]	1983	52	220–240	6.1–12.2	0.456–0.880	0.182–0.373	0.84	0.39
Al-Sahhaf et al. [44]	1990	32	230–250	6.2–10.3	0.388–0.880	0.240–0.475	2.0	0.72
Sarashina et al. [45]	1971	53	233–273	6.1–10.1	0.543–0.95	0.25–0.725	1.1	0.94
Somait and Kidnay [46]	1978	41	270	4.6–11.1	0.665–0.971	0.587–0.789	0.72	1.41
Trappehl and Knapp [47]	1989	51	220	2–12	0.465–0.978	0.17–0.350	0.64	0.50
Xu et al. [48]	1992	53	293	6.0–8.3	0.878–0.991	0.859–0.975	0.37	0.39
This work	2019	31	223–298	0.8–9.3	0.803–0.997	0.594–0.971	0.14	0.27
***pρT* data**								
Authors	Year	N	T/K	p/MPa	z_{co_2}		AAD/%	
Magee et al. [49]	1994	39	245–400	3.5–33.1	0.960		0.11	
Seitz et al. [50]	1996	270	323–573	20–100	0.2–0.8		0.37	

An overview of the deviations in terms of mole fraction of the three components for all the experimental VLE data available in literature including the data of this work is given in Fig. 6.

To analyze the model with the data obtained in this work, more detailed deviation plots showing the residuals for each isotherm and measurement series are provided in Fig. 7.

In general, all residuals in terms of liquid mole fraction CO_2 are smaller than 0.5 mol% and all residuals in terms of vapor mole fraction CO_2 are smaller than 1 mol% from the EOS. The maximum deviations in terms of liquid mole fraction N_2 and CH_4 are 0.3 mol% and 0.2 mol%, respectively. The vapor mole fractions N_2 and CH_4 deviate by less than 0.6 mol% and 0.4 mol%, respectively, cf. Figs. A.1 to A.2 in Appendix A. This verifies that the EOS performs well for the ternary mixture. The general trends are increasing deviations with increasing pressures and mole fraction of N_2 and CH_4. As previously discussed, the models for ternary mixtures include parts from the binary-mixture models of the involved components. These were fitted to binary experimental data independently from multicomponent mixtures. Thus, analyzing trends in the residuals of the binary mixtures can explain shortcomings in the multicomponent mixture. In this case, the comparison is even more reasonable because VLE data in similar temperature and pressure ranges with the same apparatus for $CO_2 + N_2$ were measured by Westman et al. [25] and for $CO_2 + CH_4$ by Petropoulou et al. [28]. In Fig. 8 deviation plots between experimental measurements and values calculated with the EOS-CG-2019 [16] show similar trends. Only the isotherm at 223 K exhibits a different behavior, which might be due to a different pressure range of the measurements. Therefore, it can be concluded that the shortcomings in the binary models affect the ternary model in a similar way.

In Fig. 9, two exemplary pressure/composition plots including data measured in this work at the temperatures 273.17 K and 298.13 K are shown. The remaining isotherms are illustrated in Figs. A3 to A6 in Appendix A. The pressure is plotted versus the experimental (crosses) and calculated (circles) compositions. Mole fractions in terms of CO_2, N_2, and CH_4 are plotted separately. Since the ratio between total mole fractions of N_2 and CH_4 is kept approximately constant in each measurement series, these diagrams represent pseudo-binary pressure/composition-diagrams. Visualizing the measurements and the EOS predictions in this way gives useful information and illustrates important trends. Furthermore, the trends in these figures can be qualitatively compared to the binary pressure/composition-diagrams of $CO_2 + N_2$ [25] and

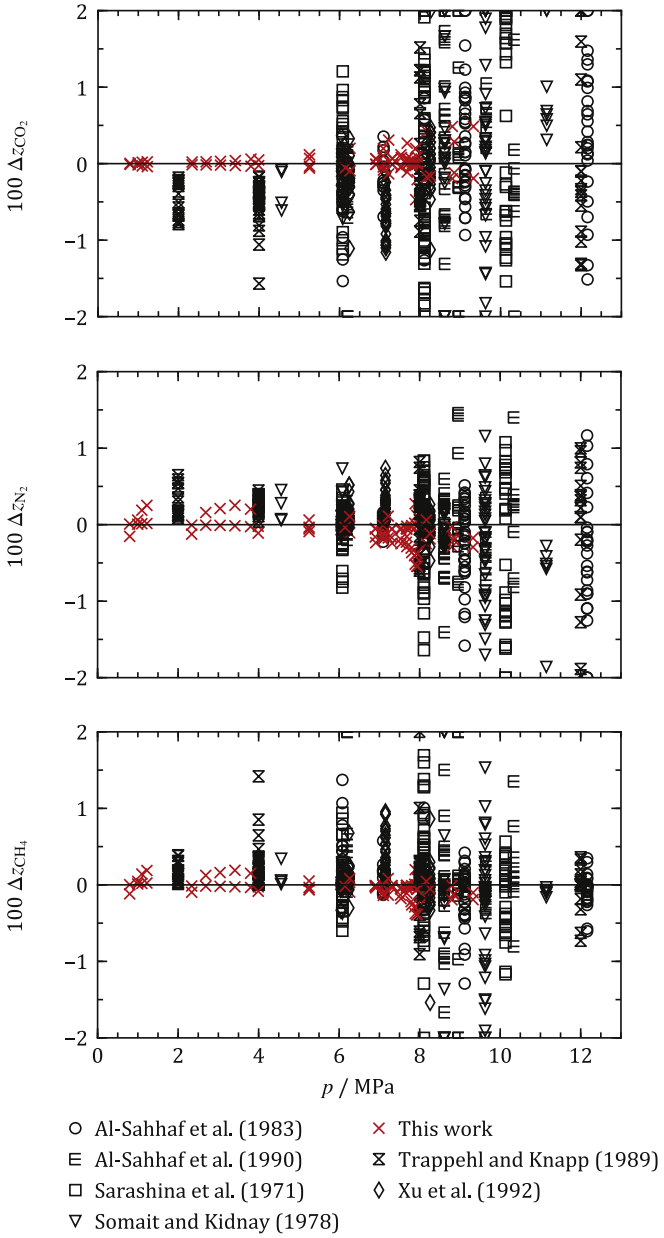

Fig. 6. Deviations between bubble- and dew-points data both from the literature [43–48] and this work and model calculations from the EOS-CG-2019 [16] model. The deviations are calculated in terms of molar composition according to $\Delta z_i = z_{i,\mathrm{exp}} - z_{i,\mathrm{calc}}$ for i equal to CO_2, N_2, and CH_4 (top to bottom).

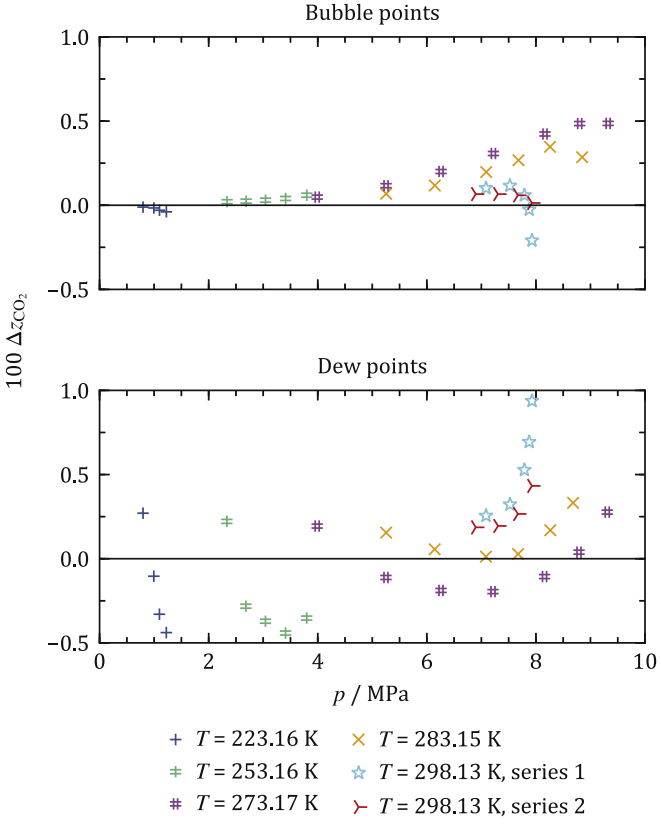

Fig. 7. Deviations between bubble- (top) and dew-point data (bottom) measured in this work and calculated with the EOS-CG-2019 [16] model. The deviations are calculated in terms of CO_2 mole fraction according to $\Delta z_{CO_2} = z_{CO_2,\mathrm{exp}} - z_{CO_2,\mathrm{calc}}$.

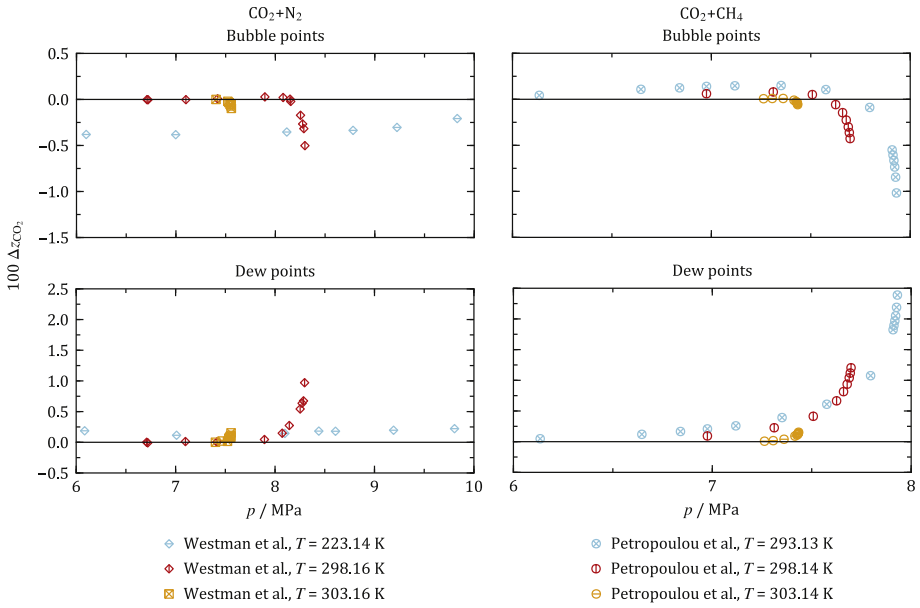

Fig. 8. Deviations between bubble- and dew-points from measurements [25,28] and calculated with the EOS-CG-2019 [16] model for binary mixtures of $CO_2 + N_2$ and $CO_2 + CH_4$. The deviations are calculated in terms of molar composition according to $\Delta z_{CO_2} = z_{CO_2,exp} - z_{CO_2,calc}$.

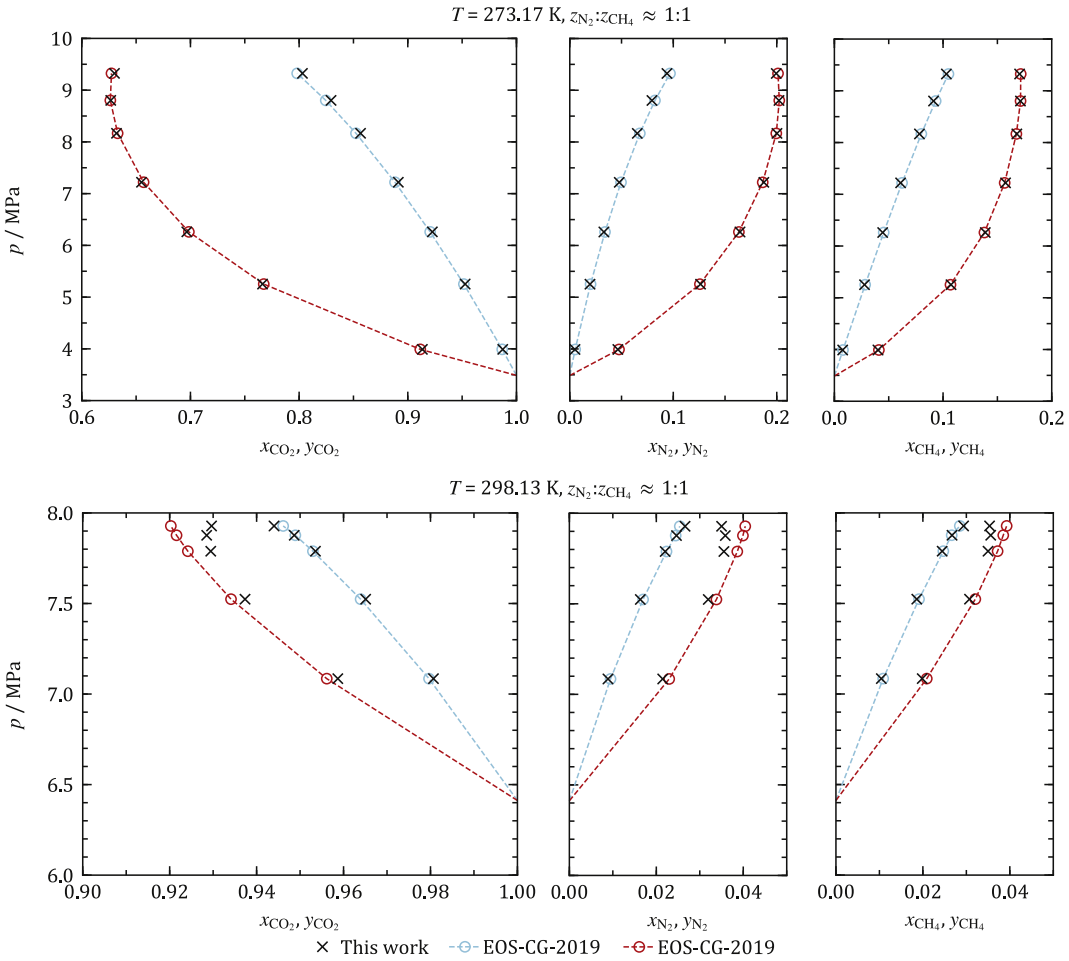

Fig. 9. Comparisons of the experimental VLE data points measured in this work (top: L16 – L22 and V16 – V22, bottom: L1 – L5 and V1 – V5) with the corresponding saturation points calculated with the EOS-CG-2019 [16] in terms of pressure versus mole fractions of CO_2, N_2, and CH_4 at the temperatures 273.17 K (top) and 298.13 K (bottom). The dashed lines are only connection lines and do not have any thermodynamic meaning.

$CO_2 + CH_4$ [28] at different temperatures. The dashed lines between the points calculated with the EOS do not represent the model or the phase boundary but are straight lines between the model points in order to support the visualization.

Fig. 9 illustrates that the model reproduces the phase boundaries well for lower temperatures. Although the deviations on the dew line are higher than on the bubble line (see Fig. 7) the qualitative representation is good. The data starts to deviate more for higher pressures at 283 K, cf. Fig. A.5, which continues for increasing temperatures. However, it has to be noted that the composition range on the x-axis for 298 K is smaller than for 273 K. Thus, absolute deviations have to be evaluated carefully. The trend of the residuals for the ternary mixture follows the trend of the binary mixtures at higher pressures as can be seen in Fig. 8. For the binary systems $CO_2 + N_2$ and $CO_2 + CH_4$ as well as the ternary system the model underestimates the mole fraction of CO_2 and overestimates the mole fractions of N_2 and CH_4 for higher pressures, which is for example visible at the 298 K measurements. As a result, the calculated deviations between the model and the data do not fully comply with the estimated experimental uncertainties in Tables 2 and 3 Nevertheless, the phase boundaries are described qualitatively well, considering the predictive nature of the model.

The publications of Al-Sahhaf et al. [43,44] state uncertainties for temperature, pressure, and composition measurements but no combined experimental uncertainty. Since in this work the deviations are calculated in terms of composition, the accuracy of the composition measurement (±0.2 mol% [43] and ±0.3 mol% [44]) is the best indication for any comparisons. Considering that temperature and pressure uncertainties will increase a combined uncertainty and that the common confidence level of 95% ($k = 2$) has to be applied, most of the data are represented within the experimental uncertainty. Fig. 10 shows the description of the phase boundaries in a ternary composition diagram. The dew-point data are represented more accurately than the bubble-point data, which is also indicated by the AAD in Table 8.

Sarashina et al. [45] do not state any uncertainties. Thus, it is difficult to evaluate the EOS with the data. Nevertheless, most of data are represented within 1 mol%.

Somait and Kidnay [46] measured 41 data points at 270 K and five different pressures. The reported uncertainties of the temperature, pressure, and composition measurements are ±0.02 K, ±0.015 MPa, and ±0.2 mol%, respectively. But no combined experimental uncertainty is stated. Moreover, the data also do not show the miscibility gap at $T = 270$ K and $p = 8.61$ MPa towards the binary mixture of CO_2 and CH_4.

The VLE data provided by Trappehl and Knapp [47] are difficult to evaluate because neither a description of the experimental apparatus nor measurement uncertainties are given. Nevertheless, Al-Sahhaf et al. [43] agrees well with these data (see Fig. 10) and the AAD for both phases are well below 1 mol%.

Xu et al. [48] measured 53 VLE data points at 293 K and four different pressures. The authors state experimental uncertainties of ±0.01 K in terms of temperature, ±0.02 MPa in terms of pressure, and ±0.1 mol% in terms of composition. The purities of the pure components were better than 99.95%. No combined expanded uncertainty is given. The EOS accurately describes the data with an AAD of less than 0.4 mol% in terms of CO_2 mole fraction and maximum deviations of 1.2 mol% (dew point measurements) and 1.1 mol% (bubble point measurements).

4.2.2. Comparisons to homogeneous density data

Only two publications report densities for this ternary mixture. Seitz et al. [50] measured vapor and liquid densities in temperature and pressure ranges from 323 K to 573 K and from 20 MPa to 100 MPa, respectively, with “a custom-designed vibrating-tube densimeter”. The mole fractions are distributed between 10 mol% and 80 mol % for each component resulting in a total number of 270 state points. The stated uncertainties for pressure and temperature are ±0.02 MPa and ±0.05 K. The purities of the compounds are better than 0.9999 in terms of mass fraction. The estimated uncertainty in terms of density is less than $\pm 1 \mathrm{kg \cdot m^{-3}}$. However, it is not described how this value was calculated. There is also no indication that the uncertainty in composition was taken into account. Thus, the estimated uncertainty has to be higher. Converting only the density specification estimate into a relative uncertainty, the average relative uncertainty is 0.34% with a maximum of 1.03%. Although the model is purely predictive, 96% of the data points deviate within the maximum uncertainty and the AAD (0.37%) is close to the average relative uncertainty. Seitz [51] performed density measurements for the pure CO_2 and CH_4 components with the same apparatus. The AAD calculated with the reference EOS [6,40] is 0.16% for CO_2 and 1.11% for CH_4. Therefore, the uncertainty

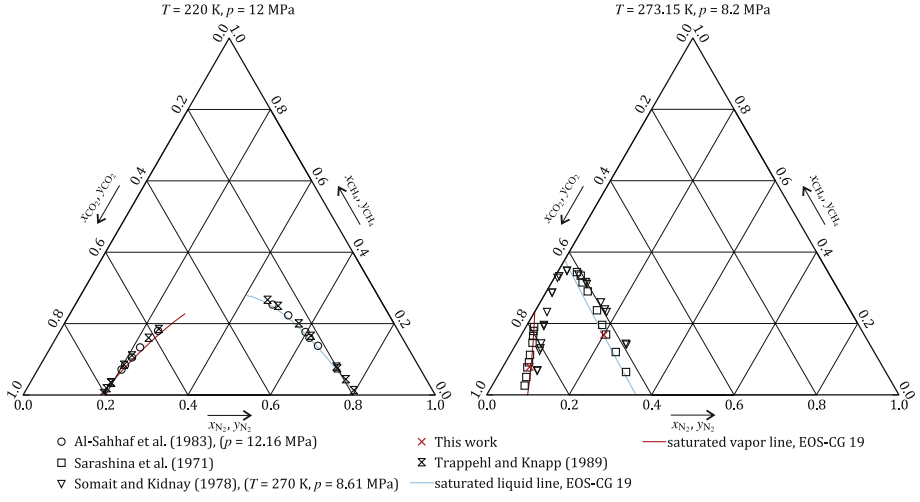

Fig. 10. Ternary phase diagrams for two different state points including the available experimental data [43,45–47].

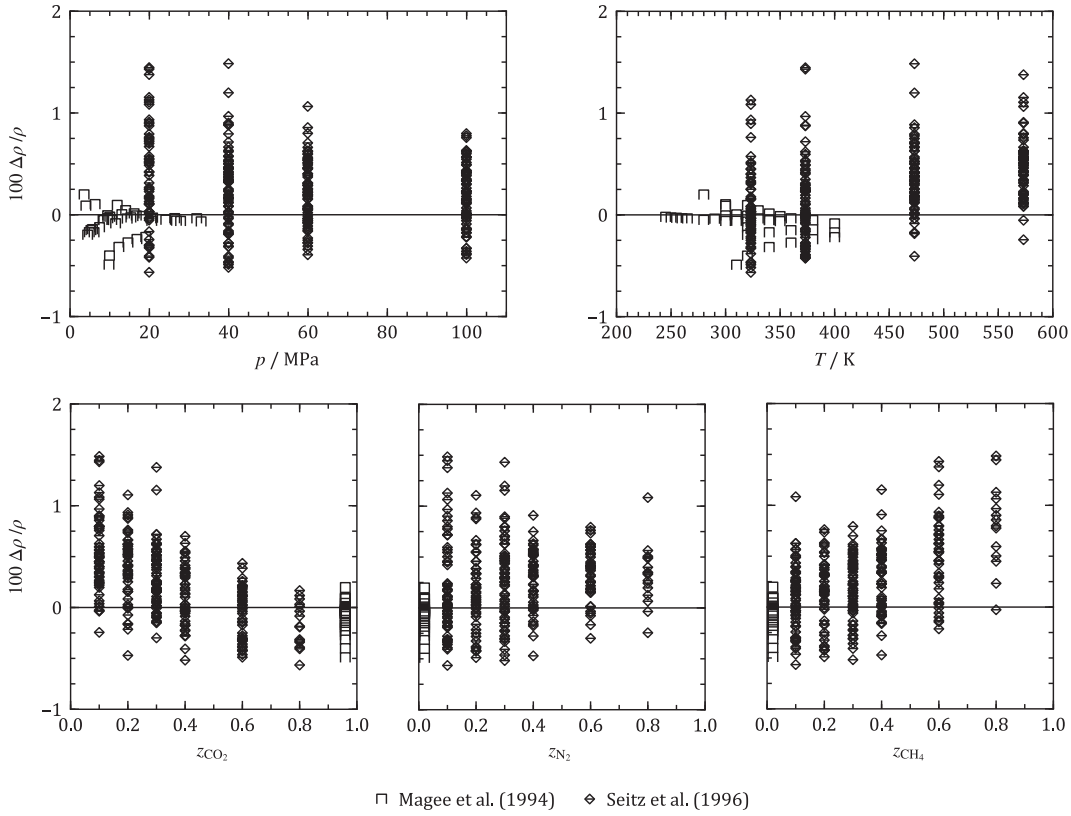

Fig. 11. Percentage deviations $\Delta\rho/\rho = (\rho_{exp} - \rho_{calc})/\rho_{exp}$ between calculated and measured homogeneous densities [49,50] as a function of pressure (top left), temperature (top right), mole fractions of CO_2 (bottom left), N_2 (bottom center), and CH_4 (bottom right).

estimates for the mixture are reasonable. The deviations with respect to pressure, temperature, and composition are shown in Fig. 11. For higher pressures, the deviations decrease slightly. There is no trend with respect to temperature. The deviations with respect to composition are decreasing for higher CO_2 and N_2 concentrations and show an opposite behavior for CH_4. However, all deviations are within the estimated experimental uncertainty. Therefore, the models perform very well.

Magee et al. [49] carried out isochoric density measurements for one CO_2-rich composition ($z_{CO_2} = 96$ mol%) with a total number of 39 data points. The reported uncertainty in temperature is ±0.03 K. The uncertainty in pressure is expressed by a polynomial function with 0.31% at 1.7 MPa to 0.019% at 35 MPa. The authors estimated a combined uncertainty of ±0.1% for the density measurements. More than 50% of the data points are within the estimated uncertainty, which is also expressed by an AAD of 0.11%. However, the maximum deviation is around 0.5%. In Fig. 11, a trend of increasing deviation with decreasing pressure is visible, which is in accordance with the trend in the pressure measurement uncertainty.

In summary, the model describes the experimental data accurately. Most of the homogeneous density data are represented within their experimental uncertainty. Thus, improving the binary-mixture models is not necessary with regard to density data. The phase boundaries calculated with the model are in accordance with VLE data measured in this work and found in the literature. However, there are shortcomings for increasing pressure at higher temperatures. New data at even higher pressures would be needed to check whether this trend continues. Moreover, other experimental thermophysical-property data, e.g. speed of sound data, would certainly allow a more comprehensive validation of the model.

5. Conclusions

Carbon capture and storage (CCS) is a necessary part of a sustainable future, but large-scale CCS deployment will require improved models for properties of relevant CO_2-fluids at conditions expected in the various processes involved. The needed reference property models generally rely on high-quality experimental data of pure components and binary mixtures. However, in order to verify that the fluid models perform sufficiently well for real process fluids, they should be tested against experimental data from mixtures with more than two components. In this work, the thermodynamics of the ternary $CO_2 + N_2 + CH_4$ mixture system has been investigated.

62 different bubble or dew points at 5 different temperatures between 223 K and 298 K have been accurately experimentally determined. The vapor-liquid equilibria were measured using the analytic method and a facility where both design and procedures are specifically developed to produce accurate data for CCS relevant fluids. The experimentally investigated temperature and pressure ranges include the technologically important low temperature − low pressure region for early or small-scale value chain utilizing vessel transport as well as the higher temperature − higher pressure domain relevant for pipeline transport.

The new VLE data and literature data on VLE and volumetric properties of the system were compared with the EOS-CG-2019 model. The equations of state in terms of the Helmholtz energy within the EOS-CG-2019 are developed specifically for CCS. In general, the deviations between the experimental data and model were small and of the same order of magnitude as the deviations between the EOS-CG and the binary data sets $CO_2 + N_2$ and $CO_2 + CH_4$. Although no new fitting of the EOS-CG was performed,

the clearly smallest residuals between model and measurements were found for the new data produced in the current work, with average absolute relative deviations (AAD) in terms of CO_2 mole fraction of 0.14% for the liquid phase and 0.27% for the vapor phase. The model also shows a reasonable and accurate behavior with regard to homogeneous densities. Hence, the predictive nature of the ternary model built on binary pure component EOS and binary mixture models fitted to data can be confirmed for the investigated range and components. Nevertheless, data in yet uncovered regions and also different thermophysical properties, e.g. heat capacity or speed of sound would certainly enhance the validation of the model.

However, this conclusion cannot in general be extended to other components without further investigations, and considerably more high-quality multicomponent data are needed for verification of thermodynamic models for CCS. The multicomponent mixture performance should of course be investigated independently for each model before being put into use for critical processes.

With regard to EOS-CG-2019, the best way to improve its performance for the $CO_2 + N_2 + CH_4$ system further is probably to refit the binary mixture models for $CO_2 + N_2$ and $CO_2 + CH_4$ taking into account new, accurate experimental data, and perhaps with an increased emphasis on the critical region. Due to the large experimental data base for these two binary systems, and for compatibility reasons, refitting these mixture models would however be a major undertaking.

Declaration of competing interest

The authors declare that they have no known competing financial interests or personal relationships that could have appeared to influence the work reported in this paper.

CRediT authorship contribution statement

Sindre Ottøy: Software, Methodology, Validation, Formal analysis, Investigation, Data curation, Writing - original draft, Writing - review & editing, Visualization. **Tobias Neumann:** Software, Validation, Formal analysis, Data curation, Writing - original draft, Writing - review & editing, Visualization, Supervision. **Hans Georg Jacob Stang:** Conceptualization, Methodology, Validation, Investigation, Supervision. **Jana Poplsteinova Jakobsen:** Supervision. **Anders Austegard:** Software, Data curation, Supervision. **Sigurd Weidemann Løvseth:** Conceptualization, Methodology, Validation, Formal analysis, Data curation, Writing - original draft, Writing - review & editing, Visualization, Supervision, Project administration, Funding acquisition.

Acknowledgements

This publication has been produced with support from the NCCS Centre, performed under the Norwegian research program Centres for Environment-friendly Energy Research (FME). The authors acknowledge the following partners for their contributions: Aker Solutions, ANSALDO Energia, CoorsTek Membrane Sciences, EMGS, Equinor, Gassco, KROHNE, Larvik Shipping, Lundin, Norcem, Norwegian Oil and Gas, Quad Geometrics, Shell, TOTAL, Vår Energi, and the Research Council of Norway (257579/E20).

Appendix A

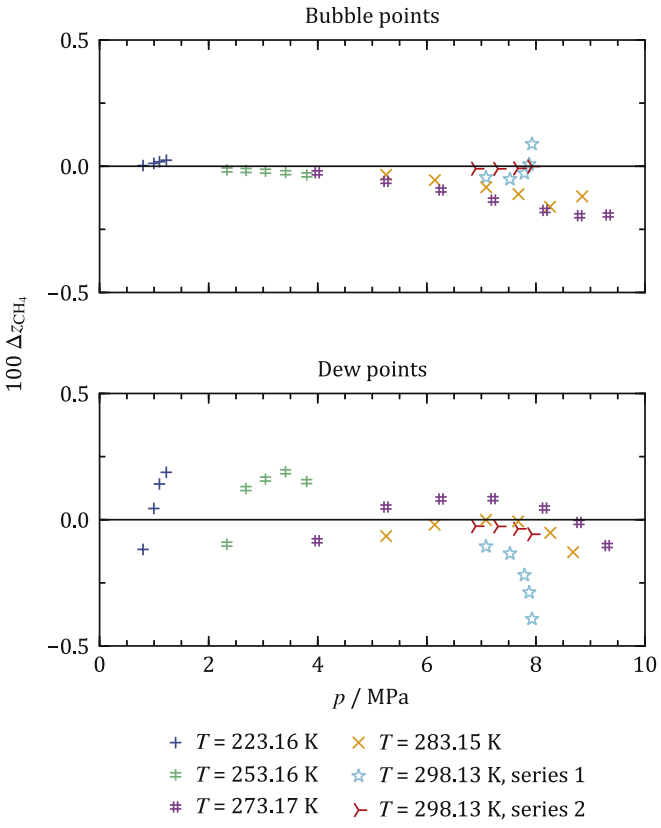

Fig. A.1. Deviations between bubble- (top) and dew-point data (bottom) measured in this work and calculated with the EOS-CG-2019 [16] model. The deviations are calculated in terms of CH_4 mole fraction according to $\Delta z_{CH_4} = z_{CH_4,exp} - z_{CH_4,calc}$.

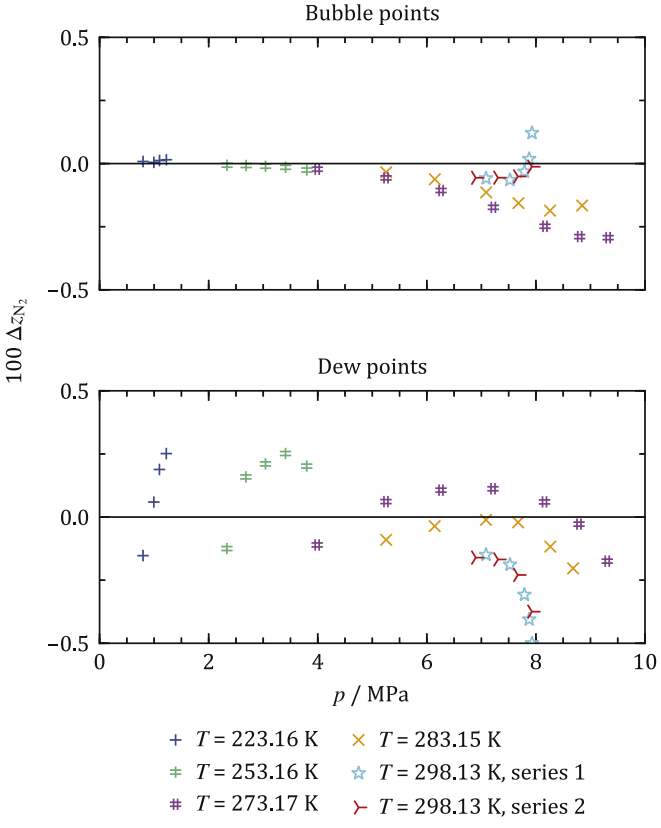

Fig. A.2. Deviations between bubble- (top) and dew-point data (bottom) measured in this work and calculated with the EOS-CG-2019 [16] model. The deviations are calculated in terms of N2 mole fraction according to $\Delta z_{N_2} = z_{N_2,exp} - z_{N_2,calc}$.

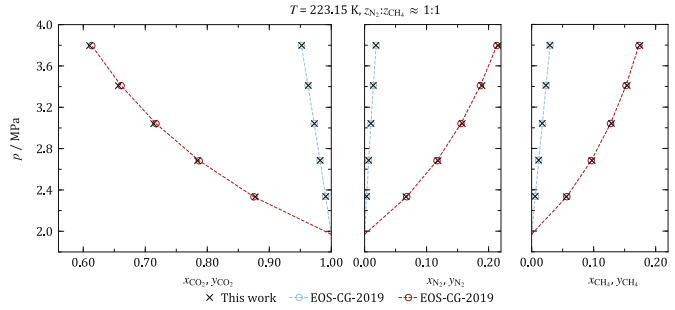

Fig. A.3. Comparisons of the experimental VLE data points measured in this work (L28 − L31 and V28 − V31) with the corresponding saturation points calculated with the EOS-CG-2019 [16] in terms of pressure versus CO_2, N_2, and CH_4 mole fractions at the temperature 223.15 K. The dashed lines are only connection lines and do not have any thermodynamic meaning.

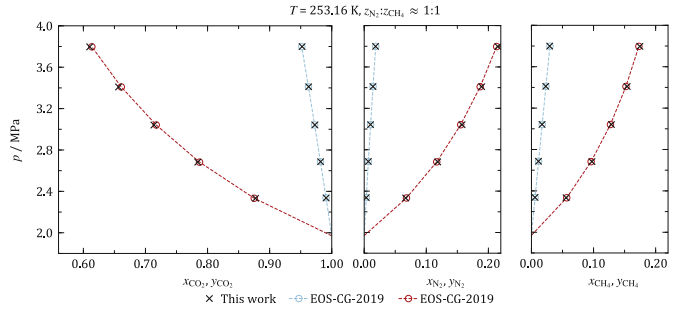

Fig. A.4. Comparisons of the experimental VLE data points measured in this work (L23 − L27 and V23 − V27) with the corresponding saturation points calculated with the EOS-CG-2019 [16] in terms of pressure versus CO_2, N_2, and CH_4 mole fractions at the temperature 253.16 K. The dashed lines are only connection lines and do not have any thermodynamic meaning.

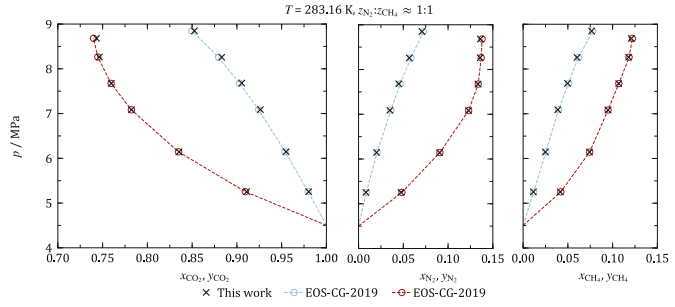

Fig. A.5. Comparisons of the experimental VLE data points measured in this work (L10 − L15 and V10 − V15) with the corresponding saturation points calculated with the EOS-CG-2019 [16] in terms of pressure versus CO_2, N_2, and CH_4 mole fractions at the temperature 283.16 K. The dashed lines are only connection lines and do not have any thermodynamic meaning.

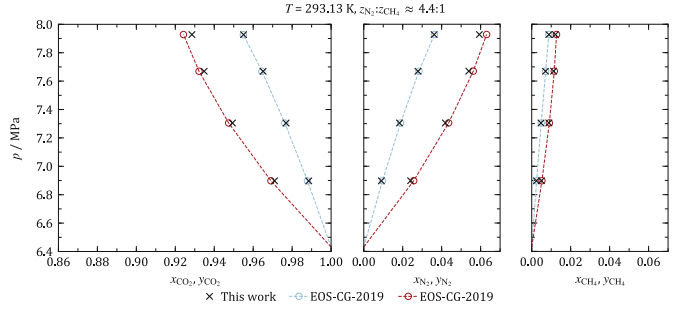

Fig. A.6. Comparisons of the experimental VLE data points measured in this work (L6 - L9 and V6 − V9) with the corresponding saturation points calculated with the EOS-CG-2019 [16] in terms of pressure versus CO_2, N_2, and CH_4 mole fractions at the temperature 293.13 K. The dashed lines are only connection lines and do not have any thermodynamic meaning.

References

[1] Energy Technology Perspectives 2017 – Catalysing Energy Technology Transformations, International Energy Agency, Paris, France, 2017 available at: http://www.iea.org/etp/.

[2] Paris agreement, United Nations, United Nations framework convention on climate change, in: https://unfccc.int/process-and-meetings/the-paris-agreement/the-paris-agreement, 2015.

[3] Global warming of 1.5°C, IPCC, https://www.ipcc.ch/sr15/, 2018.

[4] The full-scale CCS project in Norway of Work, Gassnova SF, https://ccsnorway.com/.

[5] S.T. Munkejord, M. Hammer, S.W. Løvseth, CO_2 transport: data and models − a review, Appl. Energy 169 (2016) 499−523, https://doi.org/10.1016/j.apenergy.2016.01.100.

[6] R. Span, W. Wagner, A new equation of state for carbon dioxide covering the fluid region from the triple-point temperature to 1100 K at pressures up to 800 MPa, J. Phys. Chem. Ref. Data 25 (1996) 1509−1596.

[7] A. Jäger, R. Span, Equation of state for solid carbon dioxide based on the Gibbs free energy, J. Chem. Eng. Data 57 (2012) 590−597, https://doi.org/10.1021/je2011677.

[8] A. Austegard, E. Solbraa, G.D. Koeijer, M.J. Mølnvik, Thermodynamic models for calculating mutual solubilities in H_2O−CO_2−CH_4 mixtures, Chem. Eng. Res. Des. 84 (2006) 781−794.

[9] M. Ahmad, S. Gersen, Water solubility in CO_2 mixtures: experimental and modelling investigation, Energy Proc. 63 (2014) 2402−2411, https://doi.org/10.1016/j.egypro.2014.11.263.

[10] Y. Xiang, Z. Wang, X. Yang, Z. Li, W. Ni, The upper limit of moisture content for supercritical CO_2 pipeline transport, J. Supercrit. Fluids 67 (2012) 14−21, https://doi.org/10.1016/j.supflu.2012.03.006.

[11] G. de Koeijer, J. Henrik Borch, M. Drescher, H. Li, Ø. Wilhelmsen, J. Jakobsen, CO_2 transport−Depressurization, heat transfer and impurities, Energy Proc. 4 (2011) 3008−3015, https://doi.org/10.1016/j.egypro.2011.02.211.

[12] K.Y. Song, R. Kobayashi, The water content of a carbon dioxide-rich gas mixture containing 5.31 Mol % methane along the three-phase and supercritical conditions, J. Chem. Eng. Data 35 (1990) 320−322, https://doi.org/10.1021/je00061a026.

[13] H. Li, J.P. Jakobsen, J. Stang, Hydrate formation during CO_2 transport: predicting water content in the fluid phase in equilibrium with the CO_2-hydrate, Int. J. Greenh. Gas Control 5 (2011) 549−554, https://doi.org/10.1016/j.ijggc.2010.04.013.

[14] G. Skaugen, S. Roussanaly, J. Jakobsen, A. Brunsvold, Techno-economic evaluation of the effects of impurities on conditioning and transport of CO_2 by pipeline, Int. J. Greenh. Gas Control 54 (2016) 627−639, https://doi.org/10.1016/j.ijggc.2016.07.025. Part 2.

[15] S.W. Løvseth, G. Skaugen, H.G. Jacob Stang, J.P. Jakobsen, Ø. Wilhelmsen, R. Span, R. Wegge, CO_2Mix project: experimental determination of thermo physical properties of CO_2-rich mixtures, Energy Proc. 37 (2013) 2888−2896, https://doi.org/10.1016/j.egypro.2013.06.174.

[16] S. Herrig, New Helmholtz-Energy Equations of State for Pure Fluids and CCS-Relevant Mixtures, Doktor-Ingenieur thesis, Ruhr-Universität Bochum, 2018.

[17] H. Li, B. Dong, Z. Yu, J. Yan, K. Zhu, Thermo-physical properties of CO_2 mixtures and their impacts on CO_2 capture, transport and storage: progress since 2011, Appl. Energy 255 (2019) 113789, https://doi.org/10.1016/j.apenergy.2019.113789.

[18] S.W. Løvseth, H.G.J. Stang, A. Austegard, S.F. Westman, R. Span, R. Wegge, Measurements of CO_2-rich mixture properties: status and CCS needs, Energy Proc. 86 (2016) 469−478, https://doi.org/10.1016/j.egypro.2016.01.048.

[19] Norwegian CCS Research Centre − industry driven innovation for fast track CCS deployment of Work. https://www.sintef.no/nccs.

[20] J. Gernert, A. Jäger, R. Span, Calculation of phase equilibria for multi-component mixtures using highly accurate Helmholtz energy equations of state, Fluid Phase Equilib. 375 (2014) 209−218, https://doi.org/10.1016/j.fluid.2014.05.012.

[21] S.W. Løvseth, A. Austegard, S.F. Westman, H.G.J. Stang, S. Herrig, T. Neumann, R. Span, Thermodynamics of the carbon dioxide plus argon (CO_2 + Ar) system: an improved reference mixture model and measurements of vapor-liquid, vapor-solid, liquid-solid and vapor-liquid-solid phase equilibrium data at the temperatures 213−299 K and pressures up to 16 MPa, Fluid Phase Equilib. 466 (2018) 48−78, https://doi.org/10.1016/j.fluid.2018.02.009.

[22] L.F.S. Souza, S. Herrig, R. Span, J.P.M. Trusler, Experimental density and an improved Helmholtz-energy-explicit mixture model for (CO2 + CO), Appl. Energy 251 (2019) 113398, https://doi.org/10.1016/j.apenergy.2019.113398.

[23] T. Neumann, M. Thol, I.H. Bell, E.W. Lemmon, R. Span, Fundamental Thermodynamic Models for Mixtures Containing Ammonia, 2019.

[24] H. Jacob Stang, S.W. Løvseth, S.Ø. Størset, B. Malvik, H. Rekstad, Accurate measurements of CO_2 rich mixture phase equilibria relevant for CCS transport and conditioning, Energy Proc. 37 (2013) 2897−2903.

[25] S.F. Westman, H.G.J. Stang, S.W. Løvseth, A. Austegard, S.Ø. Størset, Vapor-liquid equilibrium data for the carbon dioxide and nitrogen (CO_2 + N_2) system at the temperatures 223, 270, 298 and 303 K and pressures up to 18 MPa, Fluid Phase Equilib. 409 (2016) 207−241, https://doi.org/10.1016/j.fluid.2015.09.034.

[26] S.F. Westman, H.G.J. Stang, S.Ø. Størset, H. Rekstad, A. Austegard, S.W. Løvseth, Accurate phase equilibrium measurements of CO_2 mixtures, Energy Proc. 51

(2014) 392–401, https://doi.org/10.1016/j.egypro.2014.07.046.
[27] S.F. Westman, H.G.J. Stang, S.W. Løvseth, A. Austegard, I. Snustad, I.S. Ertesvåg, Vapor-liquid equilibrium data for the carbon dioxide and oxygen ($CO_2 + O_2$) system at the temperatures 218, 233, 253, 273, 288 and 298 K and pressures up to 14 MPa, Fluid Phase Equilib. 421 (2016) 67–87, https://doi.org/10.1016/j.fluid.2016.04.002.
[28] E. Petropoulou, E. Voutsas, S.F. Westman, A. Austegard, H.G.J. Stang, S.W. Løvseth, Vapor - liquid equilibrium of the carbon dioxide/methane mixture at three isotherms, Fluid Phase Equilib. 462 (2018) 44–58.
[29] S.F. Westman, A. Austegard, H.G.J. Stang, S.W. Løvseth, Vapor-liquid equilibrium data for the carbon dioxide and carbon monoxide (CO2 + CO) system at the temperatures 253, 273, 283 and 298 K and pressures up to 13 MPa, Fluid Phase Equilib. 473 (2018) 37–49, https://doi.org/10.1016/j.fluid.2018.05.006.
[30] E. de Visser, C. Hendriks, M. Barrio, M.J. Mølnvik, G. de Koeijer, S. Liljemark, Y. Le Gallo, Dynamis CO2 quality recommendations, Int. J. Greenh. Gas Control 2 (2008) 478–484, https://doi.org/10.1016/j.ijggc.2008.04.006.
[31] R.T.J. Porter, M. Fairweather, M. Pourkashanian, R.M. Woolley, The range and level of impurities in CO2 streams from different carbon capture sources, Int. J. Greenh. Gas Control 36 (2015) 161–174, https://doi.org/10.1016/j.ijggc.2015.02.016.
[32] H. Li, J.P. Jakobsen, Ø. Wilhelmsen, J. Yan, PVTxy properties of CO_2 mixtures relevant for CO_2 capture, transport and storage: review of available experimental data and theoretical models, Appl. Energy 88 (2011) 3567–3579, https://doi.org/10.1016/j.apenergy.2011.03.052.
[33] O. Kunz, R. Klimeck, W. Wagner, M. Jaeschke, The GERG-2004 Wide-Range Equation of State for Natural Gases and Other Mixtures, VDI Verlag, Düsseldorf, Germany, 2007.
[34] O. Kunz, W. Wagner, The GERG-2008 wide-range equation of state for natural gases and other mixtures: an expansion of GERG-2004, J. Chem. Eng. Data 57 (2012) 3032–3091, https://doi.org/10.1021/je300655b.
[35] G.J. Gernert, Modeling CCS Systems – Available Data Sets and Requirements I: Fluid Properties and Phase Equilibria, IMPACTS Workshop, Bochum, Germany, 2013.
[36] Evaluation of Measurement Data — Guide to the Expression of Uncertainty in Measurement (GUM), JCGM, 2008.
[37] D.B. Newell, F. Cabiati, J. Fischer, K. Fujii, S.G. Karshenboim, H.S. Margolis, E. de Mirandés, P.J. Mohr, F. Nez, K. Pachucki, T.J. Quinn, B.N. Taylor, M. Wang, B.M. Wood, Z. Zhang, The CODATA 2017 values of h , e , k , and N A for the revision of the SI, Metrologia 55 (2018) L13–L16, https://doi.org/10.1088/1681-7575/aa950a.
[38] J. Gernert, R. Span, EOS-CG: a Helmholtz energy mixture model for humid gases and CCS mixtures, J. Chem. Thermodyn. 93 (2016) 274–293, https://doi.org/10.1016/j.jct.2015.05.015.
[39] M. Thol, M. Richter, E.F. May, E.W. Lemmon, R. Span, EOS-LNG, A fundamental equation of state for the calculation of thermodynamic properties of liquefied natural gases, J. Phys. Chem. Ref. Data 48 (2019), 033102, https://doi.org/10.1063/1.5093800.
[40] U. Setzmann, W. Wagner, A new equation of state and tables of thermodynamic properties for methane covering the range from the melting line to 625 K at pressures up to 100 MPa, J. Phys. Chem. Ref. Data 20 (1991) 1061–1155, https://doi.org/10.1063/1.555898.
[41] R. Span, E.W. Lemmon, R.T. Jacobsen, W. Wagner, A. Yokozeki, A reference equation of state for the thermodynamic properties of nitrogen for temperatures from 63.151 to 1000 K and pressures to 2200 MPa, J. Phys. Chem. Ref. Data 29 (2000) 1361–1433, https://doi.org/10.1063/1.1349047.
[42] R. Span, R. Beckmüller, T. Eckermann, S. Herrig, S. Hielscher, A. Jäger, E. Mickoleit, T. Neumann, S. Pohl, B. Semrau, M. Thol, TREND. Thermodynamic Reference and Engineering Data 4.0, Lehrstuhl für Thermodynamik, Ruhr-Universität Bochum, Bochum, 2019.
[43] T.A. Al-Sahhaf, A.J. Kidnay, D.E. Sloan, Liquid + vapor equilibria in the N_2 + CO_2 + CH_4 system, Ind. Eng. Chem. Fundam. 22 (1983) 372–380, https://doi.org/10.1021/i100012a004.
[44] T.A. Al-Sahhaf, Vapor—liquid equilibria for the ternary system $N_2 + CO_2 + CH_4$ at 230 and 250 K, Fluid Phase Equilib. 55 (1990) 159–172, https://doi.org/10.1016/0378-3812(90)85010-8.
[45] E. Sarashina, Y. Arai, S. Saito, Vapor-liquid equilibria for the nitrogen-methane-carbon dioxide system, J. Chem. Eng. Jpn. 4 (1971) 377–378, https://doi.org/10.1252/jcej.4.377.
[46] F.A. Somait, A.J. Kidnay, Liquid-vapor equilibriums at 270.00 K for systems containing nitrogen, methane, and carbon dioxide, J. Chem. Eng. Data 23 (1978) 301–305, https://doi.org/10.1021/je60079a019.
[47] G. Trappehl, H. Knapp, Vapour-liquid equilibria in the ternary mixture N_2-CH_4-CO_2 and the quaternary mixture N_2-CH_4-C_2H_6-C_3H_8, Cryogenics 29 (1989) 42–50, https://doi.org/10.1016/0011-2275(89)90010-6.
[48] N. Xu, J. Dong, Y. Wang, J. Shi, High pressure vapor liquid equilibria at 293 K for systems containing nitrogen, methane and carbon dioxide, Fluid Phase Equilib. 81 (1992) 175–186, https://doi.org/10.1016/0378-3812(92)85150-7.
[49] J.W. Magee, J.A. Howley, J.F. Ely, A Predictive Model for the Thermophysical Properties of Carbon Dioxie Rich Mixtures, Gas Processors Association, 1994, p. 32. RR-136.
[50] J.C. Seitz, J.G. Blencoe, R.J. Bodnar, Volumetric properties for $\{x_1CO_2+x_2CH_4+(1-x_1-x_2)N_2\}$ at the pressures (19.94, 39.94, 59.93, and 99.93) MPa and temperatures (323.15, 373.15, 473.15, and 573.15) K, J. Chem. Thermodyn. 28 (1996) 539–550, https://doi.org/10.1006/jcht.1996.0050.
[51] J.C. Seitz, Experimental Determination of the Volumetric Properties for the System CO_2-CH_4-N_2 at 100-1000 Bars and 50-300°C, PhD Thesis, Virginia Polytechnic Institute and State University, 1994.